PUBLIC PROCUREMENT NO. 255212
"PURCHASE OF ADDITIONAL STUDIES FOR IMPACT ASSESSMENT"

REPORT ON ACTIVITY 2
"Mapping the disused sealed radioactive sources and radioactive waste placed in reactor compartments and then covered with concrete in the concrete mass."

29th November 2023

GScan OÜ R&D
Tehnopargi tee 5
61715 Tõrvandi, Estonia
Reg. no. 14445579 / VAT EE102069978

AUTHORS

Tarvo Metspalu (report editor, tarvo.metspalu@gscan.eu), Andres Nurme (project manager, andres.nurme@gscan.eu), T.Uibo, V.Gulik, M.Mikkor, M.Deak, M.Kiisk, T.Lepp, A.Ingalt, J.Štubis, M.Mägi, L.Mägi, V.Pastsuk, F.Punga, A.Anier, E.Priidel, S.Nõmmiste, E.Ersoy, K.Saul, G-L. Küppas, C.Hrytsiuk, D.Hrytsiuk, A.Tammiksaar, K.Aktas and other valuable GScan employees

TABLE OF CONTENTS

ABBREVIATIONS

DAQ	Data acquisition [system]
FiBOT	Fibre laying roBOT
FoV	Field of view
GEANT	GEometry ANd Tracking [software]
HEPA	High Efficiency Particulate Air [filter]
HMS	Hodoscope Movement System
MCNPX	Monte Carlo N-Particle eXtended
MPS	Muon Parameterisation Source
MST	Muon Scattering Tomography
MTR	Muon Transmission Radiography
PSF	Plastic Scintillating Fibres
QA	Quality Assurance
RCSRC	Row-Column Summing Readout Circuit
SCD	Symmetric Charge Division
SiPM	Silicon Photomultiplier(s)
UV	Ultraviolet
VOI	Volume-of-interest

1   THE INTRODUCTION AND THE OBJECTIVES OF WORK

ALARA Ltd is a state-owned company within the jurisdiction of the Ministry of Climate. Its main activities include managing and decommissioning of the former nuclear facility in Paldiski and the Tammiku radioactive waste storage, management of radioactive waste generated in Estonia, developing and implementing projects related to the management of radioactive waste, and providing services in the measurement of radioactivity and deactivation of radioactive contamination.

The company was established in 1995 to manage and clean up the nuclear facility in Paldiski, which was taken over by the Estonian Republic from the Russian Federation in September 1995. On November 1 of the same year, the Tammiku radioactive waste storage was also transferred from the Tallinn Special Motor Base, where radioactive waste from Estonian industrial enterprises, research institutions, and medical facilities had been stored since the early 1960s.

Since 1995, extensive work has been carried out at the former nuclear facility in Paldiski to clean up contamination and adapt it to current needs. This includes the construction of a modern interim storage facility for radioactive waste in the main building of the nuclear facility, used for both on-site decommissioning and the storage of waste generated throughout Estonia. The Tammiku radioactive waste storage has been closed for waste disposal since 1995, and the final closure requires the removal of all waste stored there, a process that began in 2008.

In the early 1960s, a Soviet nuclear submarine training center was established in Paldiski, Estonia. The facility housed two training stands with operational nuclear reactors, used for training submarine crews in nuclear energy and reactor management. After a safety assessment following the Chernobyl disaster, both reactors were temporarily shut down in 1989. The facility was transferred to Estonia in 1995, and extensive cleanup and demolition work has since been conducted.

ALARA Ltd is responsible for the development and implementation of radioactive waste management projects, including at the nuclear facility of the previously mentioned former nuclear submarine training center in Paldiski. There are two reactors that GScan is measuring in Paldiski — 346A ("Old reactor") & 346B ("New reactor"), both resting on top of a steel scaffolding supported onto concrete beams. We have created physically accurate 3D models of these locations with an accuracy of around 1 cm. Both locations have rough concrete surfaces, confined entrances and confined working conditions in general

The main goal of the public procurement no. 255212 "PURCHASE OF ADDITIONAL STUDIES FOR IMPACT ASSESSMENT" is to understand the content of the reactors and lawfully dispose of radioactive waste. Most structures on the Paldiski site have been demolished, leaving only a renovated main building with modern radioactive waste storage, a control building, and a garage. Cleanup efforts, complying with safety standards, concluded in 2012, but final decommissioning activities related to reactor sections are expected to continue until 2040-2050. Before starting reactor dismantling in 2040, a permanent radioactive waste repository must be established in Estonia to accommodate waste generated during the decommissioning process. Moreover, thorough analysis of the reactors has to be carried out before dismantling, which was the task for GScan using muon transmission radiography.

2 GSCAN HARDWARE

2.1 Hodoscope and irradiation source description

Two hodoscopes (tomographic sensor blocks) – essentially cuboids – with dimensions of 1718 x 905 x 355 mm were assembled. Each weigh around 90 kg and have a power consumption of up to 150 W. These hodoscopes — named H1 and H2, respectively — were able to detect and record muons passing through the reactors 346A and 346B (described in detail in Section 5). Muons are elementary particles similar to the electron, with an electric charge of −1 e and a spin of ½, but with a much greater mass, which are also produced in the atmosphere via reactions with cosmic rays. These fundamental subatomic particles are able to penetrate thick materials, which is why they are useful to gain information on objects with large dimensions and high mass.

Both hodoscopes were powered through a long (ca 20 m) cable. Additional components were either bolted onto the case and/or profiles that go around the hodoscope (see Figure 2-1). Data from each hodoscope was saved locally and then extracted manually for safety precautions and practical reasons.
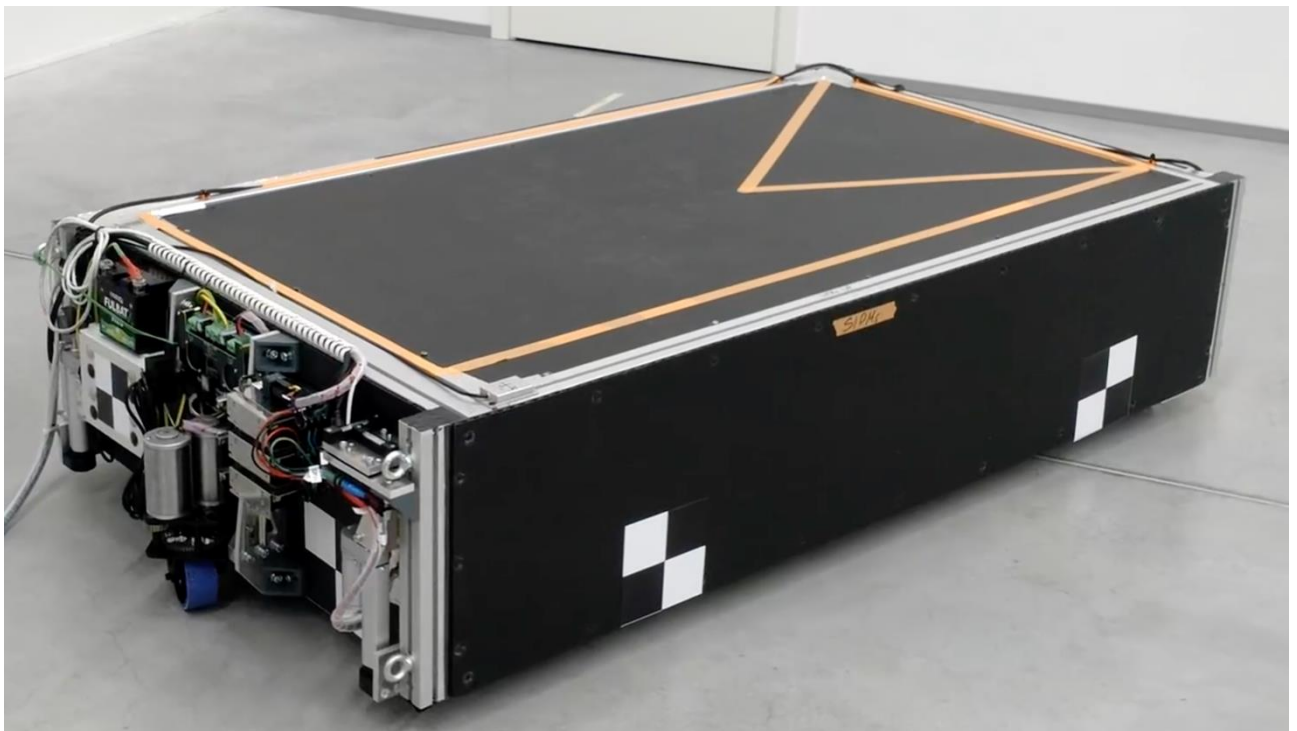

Figure 2-1. GScan's industrial hodoscope H1 with a levelling and movement system — HMS — visible on the shorter edge of the hodoscope. Positioning markers visible on the longer edge and the active area with its direction is marked on top of the hodoscope.

The following document describes the development of these unique detectors for mapping radioactive waste and other sealed sources placed in the reactor sections and then covered with concrete. This equipment was used to carry out tomographic measurements in extreme confined spaces and thus there have been a lot of challenges that have needed to be solved. If more detailed descriptions are required, please contact the main authors of this document.

2.2 **Hodoscope production**

The bulk of hodoscope's assembly consists of fiber-mats (see Figure 2-2), which are produced by aligning plastic scintillating fibres (PSF) onto composite honeycomb panels.

Figure 2-2. A fiber-mat.

From the end of December 2022 throughout February 2023 fiber-mats were produced (1538 x 768 mm ("wide") and 768 x 1538 mm ("long")) to construct a hodoscope for ALARA measurements. Six fiber-mats or three pairs of fiber-mats (3 "wide" + 3 "long") were used to assemble a hodoscope. For each pair — a detector plate — one "wide" and one "long" panel are carefully placed onto each other with fibres coming into contact perpendicularly while making sure the pressure is minimal to avoid damaging any PSF. These detector plates are thereafter distanced from one another using metal distance rods.

In general, the production can be divided into the following steps (described in detail in the "Report of Activity 1"):

1. Pre-processing of the plates

2. Automated manufacturing of fiber-mats with a proprietary robotic system FiBOT

3. Mounting the SiPMs, mirrors and multiplexing boards

4. Assembly of detector plates & hodoscope

5. Wiring and cable routing

6. QA procedures, functionality validation & diagnostics

Throughout the production process quality assurance (QA) has been done on every step of the way, including visual inspection, microscopic imaging, thermal and mechanical testing, mechanical tolerance measurements etc (see Figure 2-3). Systematic detail-oriented procedures have enabled us to optimize the FiBOT (GScan fibre-laying robot) operational parameters and modify the design of additional details (e.g., collector) on the go. Detailed mechanical analyses are not added to this report to stay within the scope – main takeaways have been implemented in the final product.

Figure 2-3. Full-scale hodoscope assembly: cabling and checking multiplexing connections

2.3 Multiplexing

To reduce the number of readout channels from the hodoscopes, an effective technique is to employ charge division (or sharing) multiplexing networks to modulate the input charge collected from the SiPM arrays. This technique routes the input charge towards output channels, and the impedance between the input channel and each of the multiplexed output channels divides the amount of input charge. As a result, the SiPMs' position and count rate information can be encoded. Typically, resistive chains are used to implement the charge division multiplexing network, which is followed by signal shaping and amplification stages at the front-end electronics module.

The hybrid symmetric charge division (SCD) network approach combines a row-column summing readout circuit (RCSRC) with a one-dimensional (1D) resistive chain or a weighted summing circuit (see Figure 2-4).
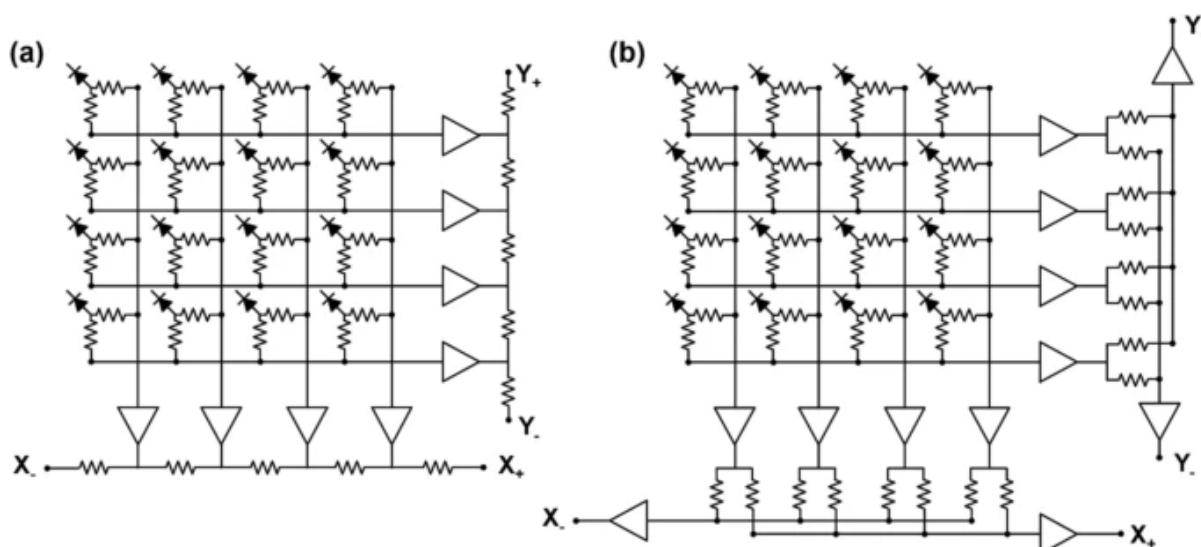

Figure 2-4. Simplified schematic of a 4x4 (16) SiPM symmetric charge division (SCD) network using: (a) 1D resistive chains ('ladders') or (b) weighted summing circuits.

In our R&D activities we are using a SiPM grid with twice the size. This means that with either diode or resistive symmetric charge division, 64 SiPMs (inputs) are clustered into 8 row channels and 8 column channels — 16 output channels in total, giving us a 64:16 or 4:1 multiplexing ratio. Each of these sixteen outputs is thereafter guided into a resistive encoding 'ladder' or a weighted summing circuit through op-amps, as seen in figure 3-1, producing 2 encoding outputs per 8 channels (XPLUS (X+) and XMINUS (X-) for row channels, YPLUS (Y+) and YMINUS (Y-) for column channels).

Final output channels are determined by applying the following ratio formula on outputs:

$$X_{position} = \frac{X_+ - X_-}{X_+ + X_-} \ , \qquad (1)$$

$$Y_{position} = \frac{Y_+ - Y_-}{Y_+ + Y_-} \ .$$

This formula outputs values between -1 and 1. Determining which channel output corresponds with which ranges will make it possible to detect which row or column channel provided the signal (see Figure 2-5).

Figure 2-5. Above. resistive encoding outputs. Red is XPLUS (X+) and blue is XMINUS (X-). Below, formula output. Each peak determines a different channel.

By combining these encoding outputs obtained from X and Y, the location of each individual SiPM can be determined.

In short, there are a lot of parameters that need to be set and optimized in order to clearly separate the signals after multiplexing. We have produced many custom iterations of multiplexing prototype boards and have now chosen a version, which should help us maximize the output of the multiplexing electronics and minimize the amount of wiring and supportive electronics from PETsys needed for data acquisition (DAQ).

3   GSCAN SOFTWARE

The following section will give background information on software for comprehension.

3.1   Particle tracking and filtering

In order to create a 3D image of the reactor (i.e., a 3D reconstruction) using natural muon flux, trajectories of muons passing the reactor compartment have to be tracked. PSF in the hodoscope can produce light (more specifically, photons) when interacting with high-energy particles like natural muons, which can then be converted into an electrical signal by SiPMs. The read-out electronics are responsible for processing and transmitting the collected data to a recorder. The data processing

Figure 3-1. A snapshot from the Geant4 detector.

algorithm is designed to search for coinciding events on multiple fiber-mats, allowing the removal of noise and non-relevant background radiation, such as gamma radiation, registered by the physical detection system.
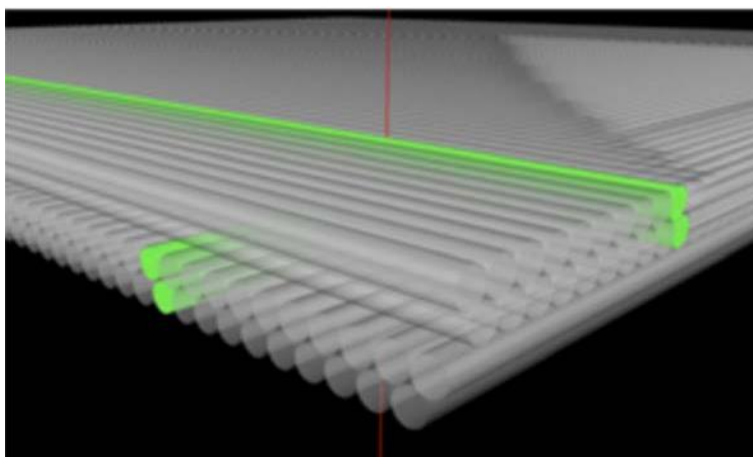
This process ensures that only events belonging to tracks of muons and other particles (such as electrons and rare protons) with cosmic ray origin are further processed. The hodoscope design provides a tracking accuracy of approximately 0.1mm and an angular accuracy of about 1 mrad.

As mentioned before, the hodoscope comprises of three detector plates, each having a four-layered structure, with two double-layered fiber-mats placed orthogonally to provide the x and y position of the particle hit. The fibre diameter measures 0.9 mm, and the pitch (distance between fibres) in a single layer is 1.0 mm. The top layer of a fiber-mat has been shifted by a half pitch and aligned in an interlocked manner based on the positions of the lower layer fibres. This guarantees close to 100% geometrical detection efficiency at every angle of incidence and a high spatial resolution. A snapshot from the
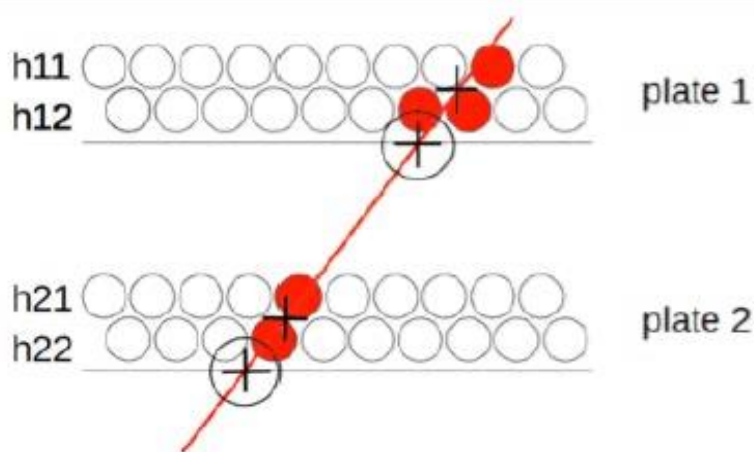

Figure 3-2. Muon trajectory extrapolation. The hxx represent PSF layers, red fibers represent fibers generating signal, the cross depicts the calculated particle hit coordinate, the circled cross indicates the extrapolated coordinates. Only two detector plates (instead of 3) with PSF for tracking one (instead of 2) axis are depicted.

Geant4 (simulation package) model of the position-sensitive detector plate is shown in Figure 3-3, composed of two double-fibre layers placed orthogonally (represented by grey cylinders), while the trajectory of a passing muon is indicated by the red line, and the propagation is illustrated by the green fibres.
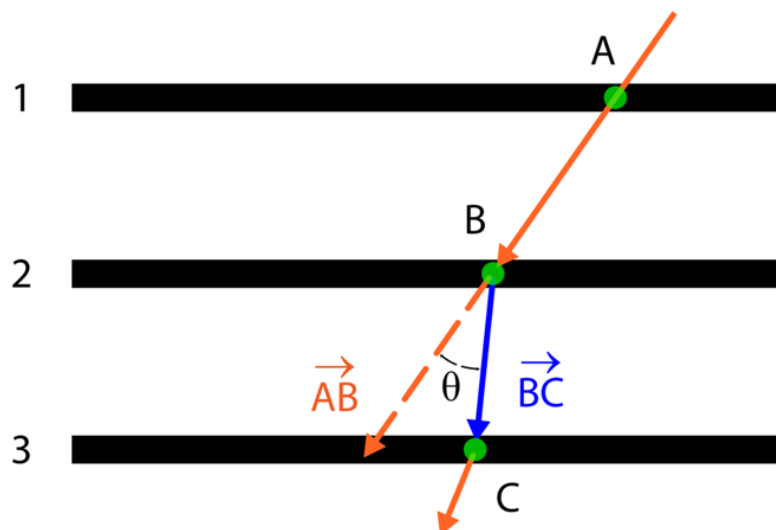

Figure 3-3. The intrinsic scattering angle θ we use to classify the particle events (passing muons/electrons) in the hodoscope. The hodoscope has the three detector plates (black bold lines numbered as 1, 2, 3). The arrows denote the reconstructed particle trajectory. The angle θ denotes the intrinsic scattering angle of the particle in the plate 2.

Adding more detector plate layers, we are able to assess in greater detail where the muons hitting (going through) the hodoscope have come from (see Figures 3-1 and 3-2).

The tracking, filtering and reconstruction is described in more detail by the authors of GScan R&D team in the article "Atmospheric ray tomography for low-Z materials: implementing new methods on a proof-of-concept tomograph", published in https://arxiv.org/abs/2102.12542.

3.2 Particle flux simulations

In order to simulate the passage of cosmic particles through the reactor compartments and develop the detector system, we use the Geant4 software. Geant4 (for GEometry ANd Tracking) is a platform for "the simulation of the passage of different particles through matter" using Monte Carlo methods. The input to cosmic-ray modelling is taken from the best suited codes, such as CRY cosmic-ray shower generator or Muon Parameterisation Source (MPS) by C.Hagmann et al.

The CRY software library generates correlated cosmic-ray particle shower distributions at one of three elevations (sea level, 2100 m, and 11300 m) for use as input to transport and detector simulation codes. CRY simulation is based on precomputed input tables derived from full MCNPX (Monte Carlo N-Particle eXtended) transport simulations of primary cosmic rays on the atmosphere and benchmarked against published cosmic-ray measurements.

CRY simulation provides all particle production (muons, neutrons, protons, electrons, photons, and pions) with the proper flux within a user-specified area and altitude. The code

generates individual showers of secondary particles sampling the energy, time of arrival, zenith angle, and multiplicity with basic correlations, and has user controls for latitude (geomagnetic cut-off) and solar cycle effects.

Figure 3-4 shows the simulation results of the filtering spectrum for the hodoscope having the distance 100 mm between the two adjacent plates. We used the CRY cosmic ray
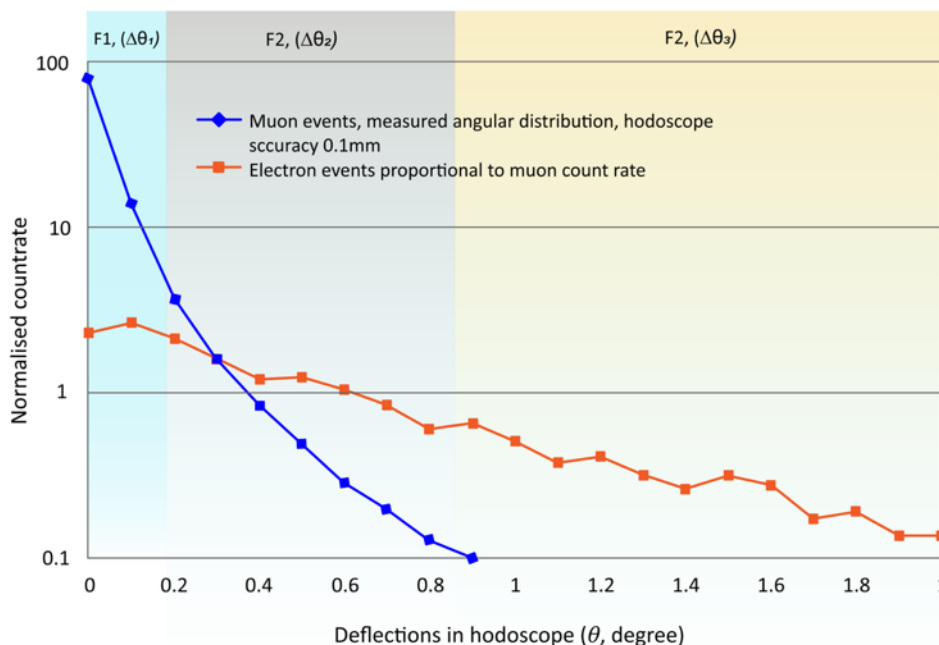

Figure 3-4. The distribution of atmospheric ray muons and electrons as a function of the intrinsic scattering angle θ in the hodoscope (from the Geant4 model with the CRY event generator). The distribution shows we can apply the intrinsic scattering angle θ as a discriminating parameter classifying the type and energy range of the hodoscope passing particle. The latter improves the tomographic reconstruction of scanned samples very significantly. The colored areas denote the muon and electron dominated values of θ (blue, yellow) and the mixed region (gray).

event generator to model the atmospheric ray flux consisting of muons and electrons at sea level. We fixed the spatial resolution of detector plates at 0.1 mm, which corresponds to the angular resolution of 1 mrad for particles approaching the hodoscope orthogonally. Considering the angular resolution of the hodoscope, the total spectral range presented in Figure 3-4 can be divided into different number of groups; we call those PTF groups below. For example, a possible robust PTF classification schema is to classify the particle events to muons and electrons or the muons with low, medium and high momentum. In Figure 3-6 we have separated the spectrum into the three PTF groups: F1 (dominated by muons), F2 (mixed muons and electrons) and F3 (dominated by electrons). This classification schema has been used in the figures of the reconstruction results in the next sections.

3.3 Reconstruction

The hodoscope measures the number of muons and their trajectories that pass through it over a certain period of time. If the measured flux is lower than expected, this indicates that the material above the detector is denser than expected, and vice versa. In addition, as we are able to track the trajectories of the muons, we can also estimate the location of these materials. The bigger the total hodoscope area, the better we can differentiate materials that are on top of each other.

INFO@GSCAN.EU

The data files obtained from each exposure position of the detector contain activation data of channels from the DAQ electronics and metadata specifying the hodoscope location in space and exposure duration. The activation data of the channels is transformed into local xyz coordinates using a tracking algorithm that improves the trajectory of the particles through the hodoscope and removes any spurious channel activations. The tracking algorithm also applies angle filtering to eliminate low-energy particles. The exposures from all detector positions are combined into a single virtual detector plane using the hodoscope positional metadata.
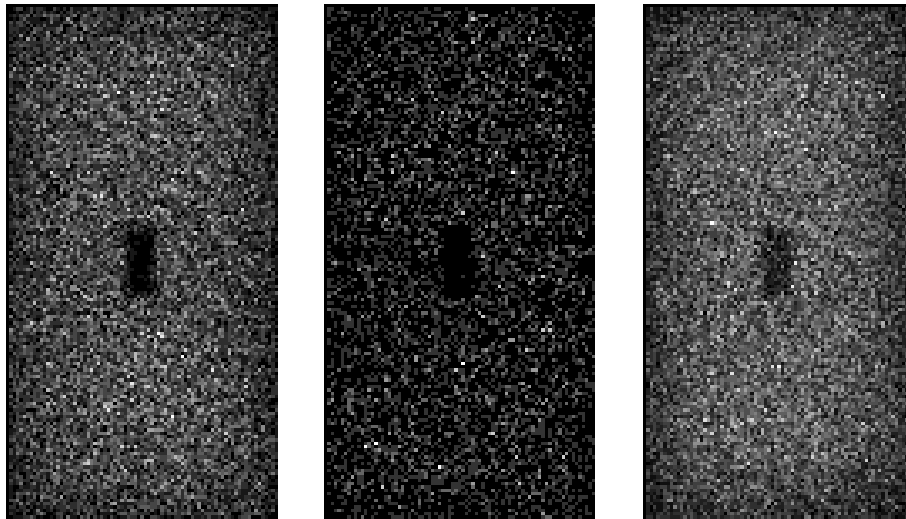
Figure 3-5. Proof-of-concept Geant4 long exposure simulation 2D cross-section results of the hodoscope with a lead brick on top in the middle.

The volume of interest (VOI), which is a limited space in which the reactor section is located, is divided into small space units called voxels with side lengths of either 1.5, 10, or 30 cm — the size of the voxel can be chosen after the measurements data has already been collected. The bigger the voxel size, the less time the reconstruction calculation takes. Thus, bigger voxel sizes are used for quick initial estimations, as the final model will be calculated using smaller voxels. A density map of the VOI is created by projecting a ray through each voxel, and each voxel that the ray passes through is given a count of +1. The 3D density map can be presented as a 3D image or 2D cross-sectional cuts/slices where voxel ray rate, after normalization, is displayed as a pixel intensity in grayscale or colored heatmap.

3.4 Analysis

GScan analytical software package is written in Python. GPU acceleration is used where applicable. Software high level functional description is as follows.

Saved data files from each detector exposure position contains channel activation data from DAQ electronics and metadata with hodoscope location in space and exposure duration. Channel activation data will be interpreted into local xyz coordinates and tracking algorithm improves particle actual trajectory through hodoscope, as well removes erroneous channel activations. After tracking algorithm angle filtering is applied to remove low energy particles. All detector position exposures will be consolidated into one large virtual detector plane using hodoscope positional metadata. Based on hodoscope two first plate xyz

Page 12 of 39

exposures the ray is projected into space (assuming the trajectory of particle), this process is GPU accelerated.

3D density map can be presented as 3D image or 2D cross-sectional cuts/slices where voxel ray rate after normalization can be presented as pixel intensity in grayscale or colored heatmap. GScan has developed analytical method for edge and object detection as well machine learning based approach. Last step allows us to generate 3D scene with all detected objects and divide these into separate logical spaces. The final product is a 3D model of reactor sections with detected objects of interest, which can be viewed with freeware programs as for example eDrawings 2022. Some screenshots of the result can be seen at the end of this report.

4   MONTE CARLO SIMULATIONS

4.1   Reconstruction results from simulations of simplified models

We have prepared a simplified model of reactor 346A in particle physic simulation software Geant4. According to our pre-project information, 2/3 of the compartment is filled with concrete. We have placed 5 objects of interest (specified in the technical specifications of the public procurement 'Purchase of additional studies for impact assessment') in accordance with their material and geometric characteristics into concrete (see the cross-section in Figure 4-1).
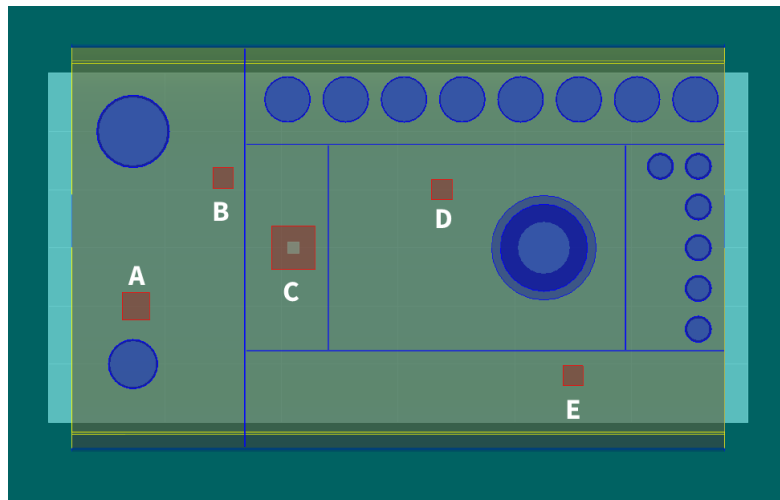
Figure 4-1. GEANT4 visualization of developed model of reactor compartment 1 with 5 hidden detectable objects: A – Lead box, B – Plastic box, C – Paraffin container, D – Stainless steel box and E – wooden box

The final measurement result at ALARA will be a 3D model of reactor sections with detected objects of interest. Additionally, we will provide cross-sectional raw data images of horizontal-cuts seen below (see Figure 4-2).
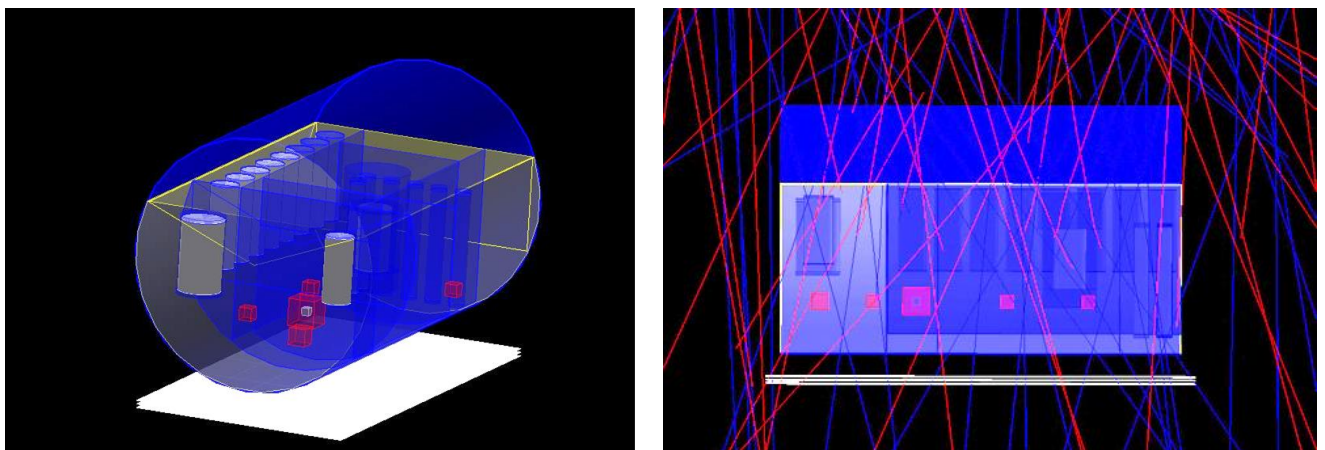

Figure 4-2. 3D Geant4 model of reactor 346A irradiated with cosmic rays.

We have previously run the described model in Geant4 simulation with 14 x 14 m CRY cosmic-ray library source for 2 hours of particle exposure time. Then we applied our proprietary software package to produce cross-sectional raw images (of reconstructed

density map). We have used two voxel sizes 1 cm on left and 5 cm on middle and right images on Figure 4-3 (the cuts are taken at the height of 5 boxes).
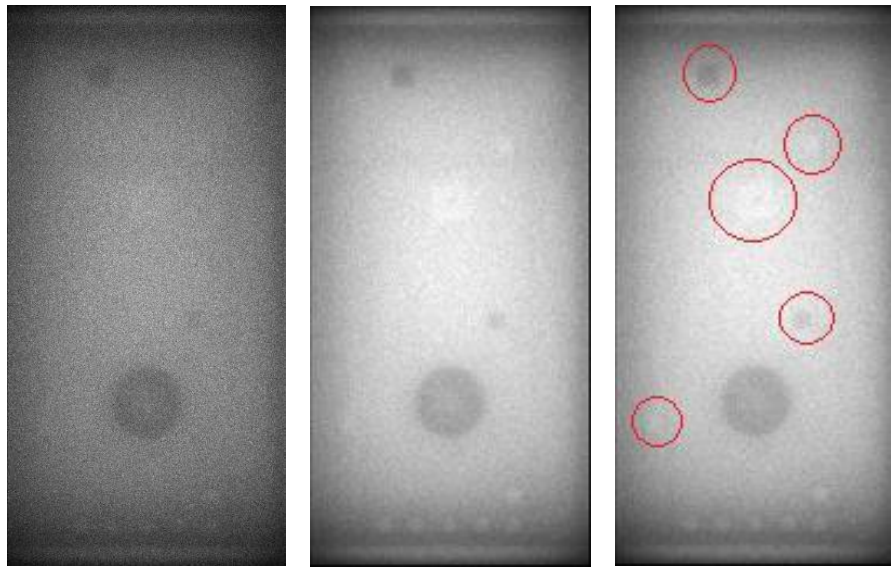

Figure 4-3. 2h of exposure in the simulation – left 1 cm voxel size; middle & right 5 cm voxel size.

While it is easier to spot all five boxes on the lower resolution image in the middle (right image is same as middle image with objects of interest circled for easy spotting), we also lose considerable detail compared to the left image. Final decision on used resolution (voxel size) will depend on measurement time available.

On Figure 4-4 there are two raw cuts from different box placement scenario (cross-sectional cuts are made at the height of metal boxes) – on the left there is 2 h exposure reconstruction and right 10 h exposure – only high energy particles were used (below 1 mrad of hodoscope internal scattering). As it can be seen, the longer exposure image provides much more sharpness and contrast due to increased statistics.
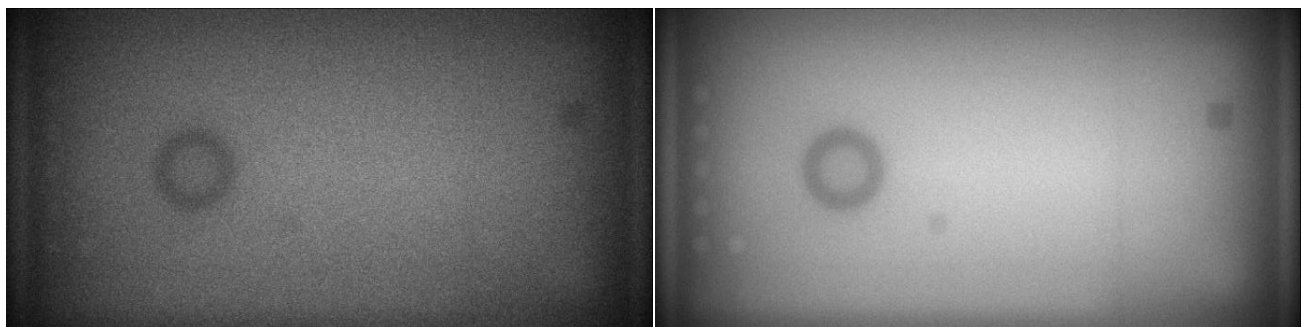

Figure 4-4. On the left, 2 h exposure simulation reconstruction and right, 10 h exposure. Notice the improved contrast and details of the image, which machine learning can easily.

Based on initial simulations it is assumed that a minimum of 12 h of exposure is required to find objects of interest (boxes defined by procurer) and other radioactive waste, but preparations are made to extend the exposures to 72 h of exposure if need be and provided time is available. Preliminary simulated data indicates that only one-sided limited angle tomographic transmission measurement suffices to achieve the set goal.

4.2 Development of improved Geant4 models

After receiving improved CAD models of the main equipment in both reactors from the customer, improved Geant4 models of both reactors (see Figure 4-5 for 346A reactor and see Figure 4-6 for 346B reactor) were developed with realistic hodoscope positions (as described in the following section) used to obtain experimental data.
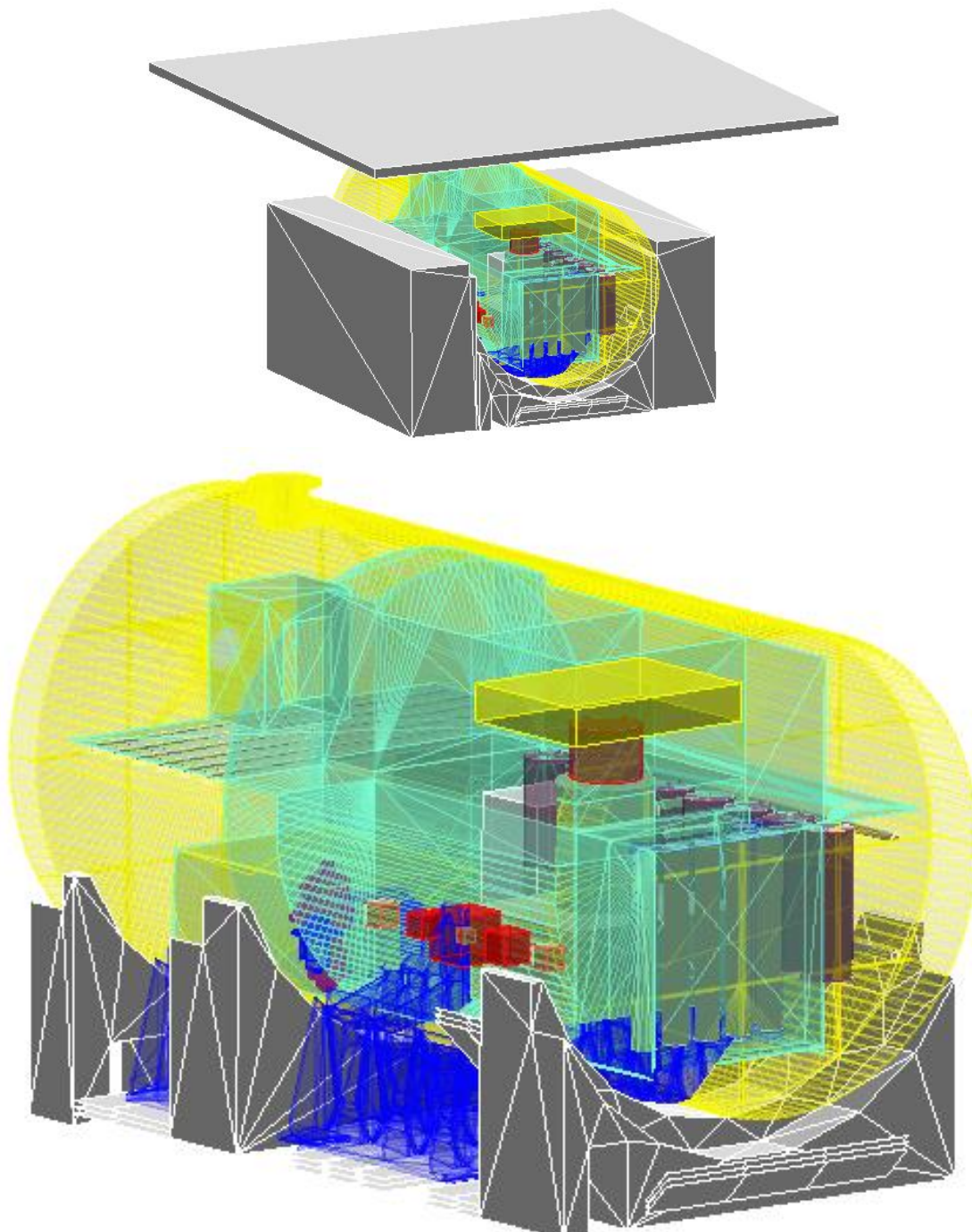

Figure 4-5. Geant4 visualization of improved model for 346A reactor. On the top, ceiling and thick concrete walls visible. Below, ceiling and thick walls have been removed.
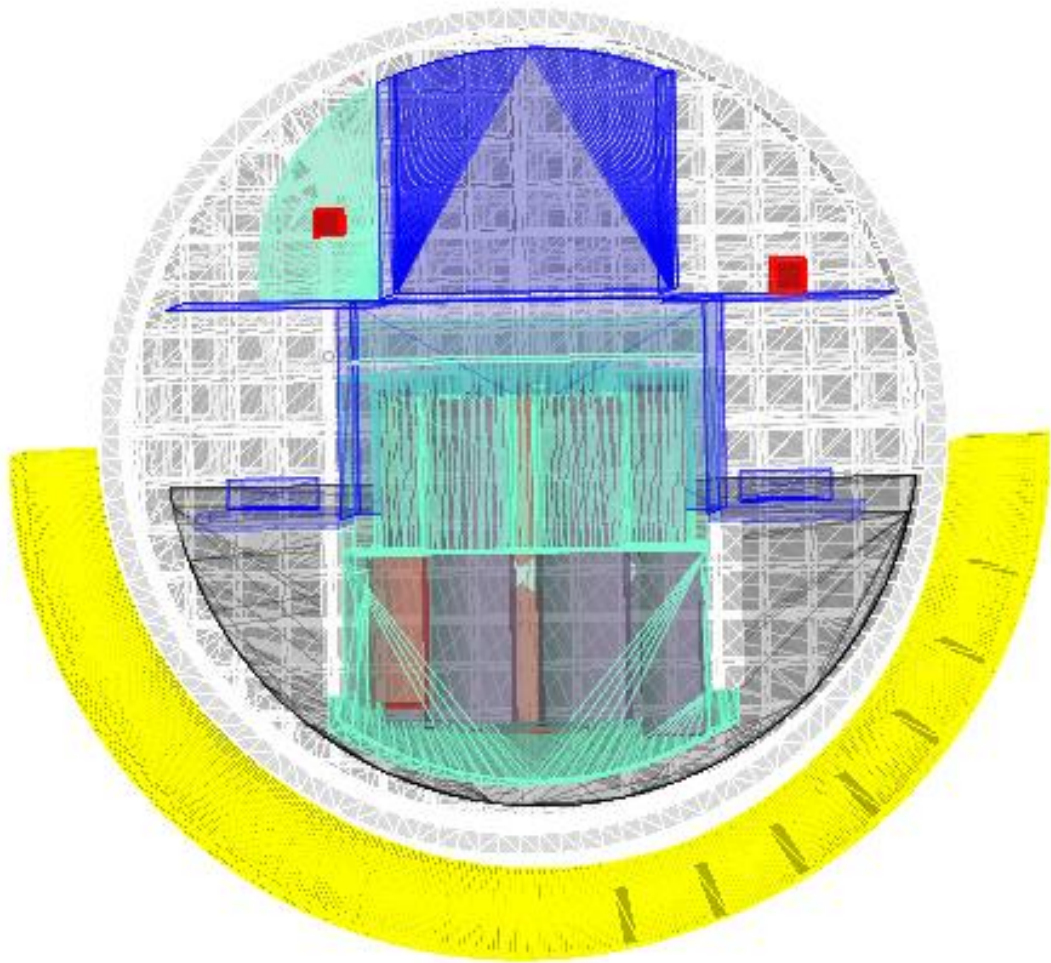
Figure 4-6. Geant4 visualization of improved model for 346B reactor.

These Geant4 models of the reactors will be used to simulate muon flux measurement results that in turn will be used for comparison with the real measurements.

5   MEASUREMENT PLANNING

5.1   346A reactor

The 346A reactor has two entrances to Front and Back sections (see Figure 5-1). The main challenge was to get the hodoscopes inside and laid on the floor (as can be seen in Figure 5-2). Therefore, no additional details could be attached outside of the measurement areas. The area of the Front (incl. support beams) is around 6.2 x 7.3 m with an average operational height of just 0.53 m. The area of the of the Back is around 2.5 x 9.5 m.
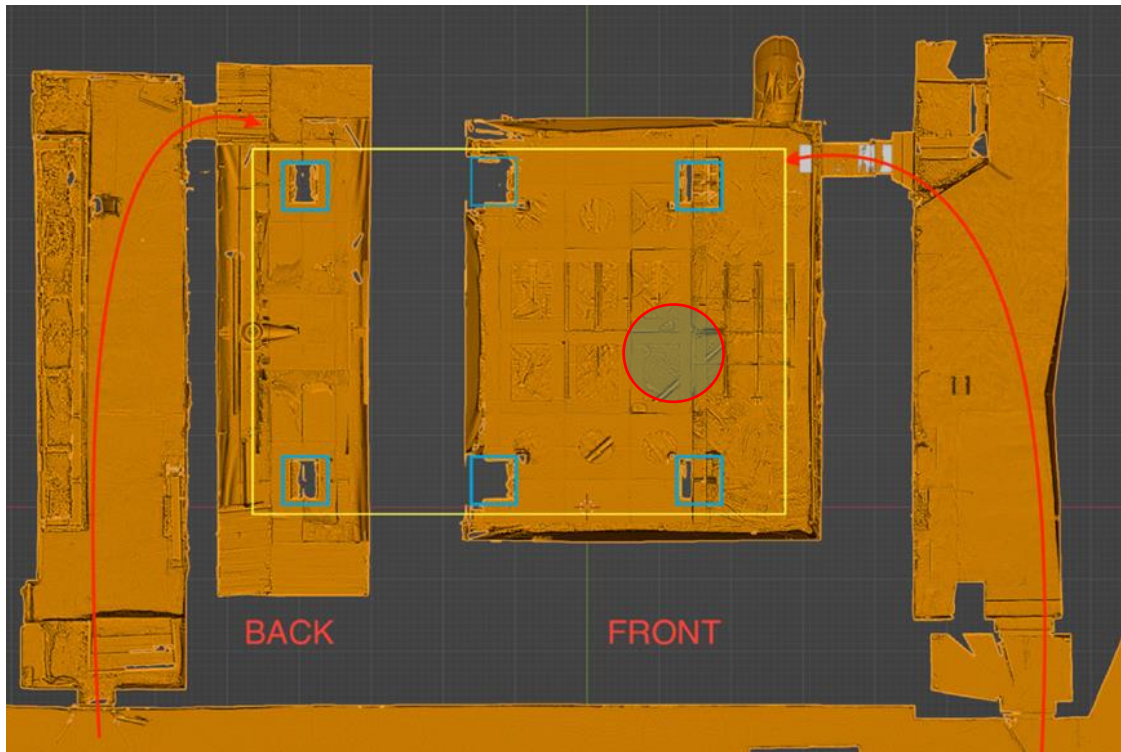

Figure 5-1. Top view of the 346A reactor 3D model with the entrance paths to the back and the front section marked with red arrows, support beams (ca 720 x 720 mm) marked with blue squares and the approximate location of the reactor on top indicated with the yellow rectangle (not true to its actual size). Notice the inaccessible areas (for the hodoscopes) between the support beams and the walls in addition to the "dead space" between the Front and the Back area. In these inaccessible areas the hodoscopes need to get as close as the wall as possible and measure for longer periods.
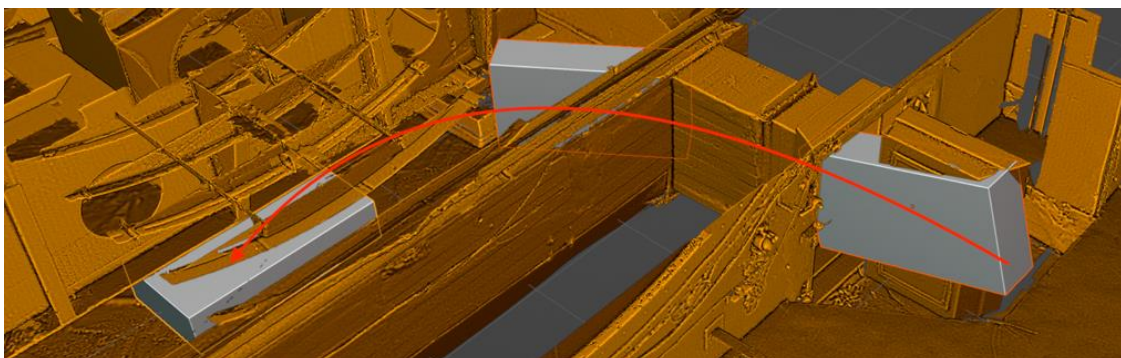

Figure 5-2. Process for guiding the hodoscope (in this case 1710 x 910 x 390 mm) underneath the 346A reactor. The measurements of the reactors are carried out by analysing muon tracks that have passed the reactor and then the hodoscope.

While the average radiation flux underneath the reactors is just a couple of times higher than the average natural flux (i.e., safe for medium periods), the middle of the Front area has a spot with higher radiation flux than the natural flux outdoors (see the red circle in Figure 5-1). This means it is highly recommended not to stay under that spot for an elongated time in order to reduce the yearly dosage a person can withstand. For safety purposes, every person got his active personal dosimeter that beeps if the flux is too high or collected dose will exceed 10 µSv.

The 346A reactor has a very uneven concrete floor surface, which increases the challenge of relocating the hodoscope under the reactor. As the reactor has been in use for a longer period, it might be also referred to as the "Old reactor".

5.2 346B reactor

The 346B reactor has a smoother concrete floor surface. Some characteristics and properties of the 346B reactor important for measurements are shown in Figure 5-3, Figure 5-4 and Figure 5-5.
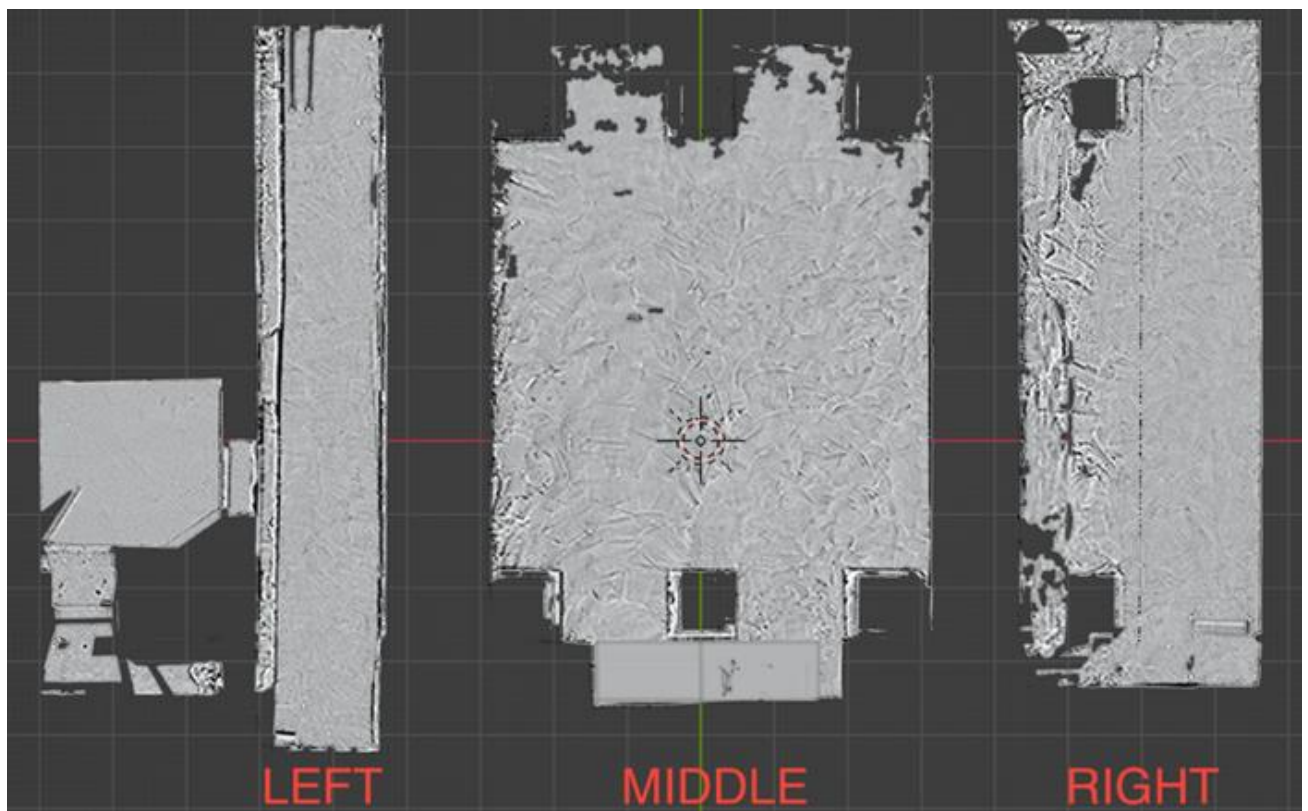

Figure 5-3. The 346B reactor can be accessed from 3 places: Left, Middle and Right.

Figure 5-4. 346B reactor Middle section floor dimensions.

Figure 5-5. Scale of the entrance (marked with red), a hodoscope (marked with green) in comparison to the 346B reactor compartment (marked with yellow). The reactor area seems hollow due to the 3D reconstruction method.

5.3 Measurement plan

With each reactor, the hodoscopes were exposed on one spot (position) after which the hodoscopes were repositioned, levelled and the location saved with the assistance of the hodoscope movement system (HMS) and/or manual labor, so the cycle could be repeated in order to cover as much (active) area with the hodoscopes underneath the reactors as possible (see Figure 5-6 and Figure 5-7, where minimum number of positions are shown). Notice that there is not enough space to place the hodoscope in some areas (e.g., near the foundation posts), thus the exposure time is increased near those areas.

Furthermore, despite these seemingly "blind spots" e.g. around the poles, the reactor is mostly "visible" to the hodoscope at all times (see Figure 5-8) as its maximum field of view (FoV) is defined by twice the maximum angle (as measured from the surface normal) of the muon trajectory passing the hodoscope. The exposure time around these "blind spots" is increased to improve normalizing the measurement results (gather more statistical data of the particle trajectories).

Figure 5-6. Measurement plan of the 346A reactor, where 47 different hodoscope measurement positions have been indicated. Some additional measurements were made at positions 1 and 2, respectively, as the initial flux was greater due to gamma rays, as previously expected.
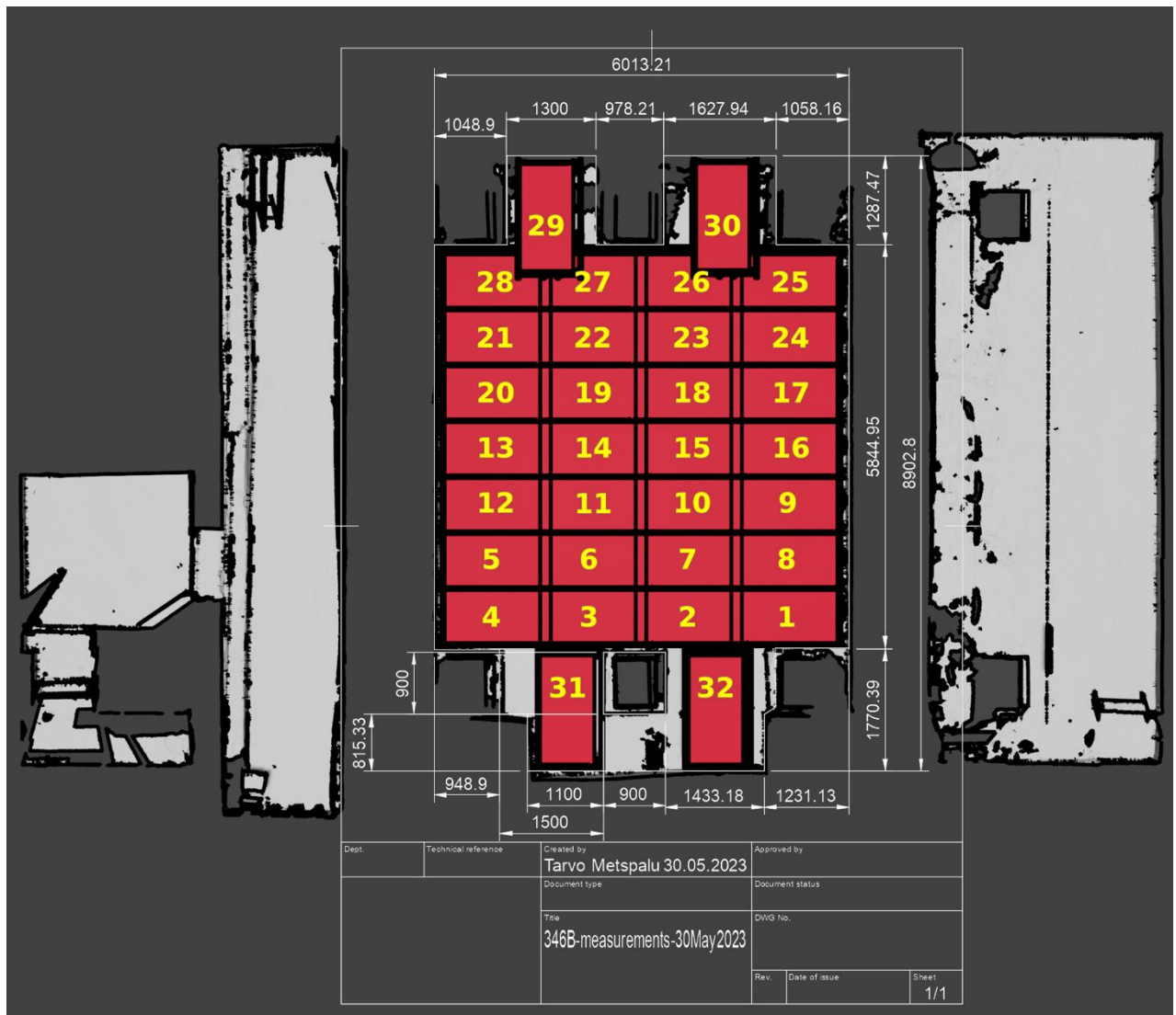
Figure 5-7. Measurement plan of the 346B reactor, where 32 different hodoscope measurement positions have been indicated. This is considered as the minimum measurement plan as most of the positions had to be re-exposed due to an initially faulty data conversion configuration.
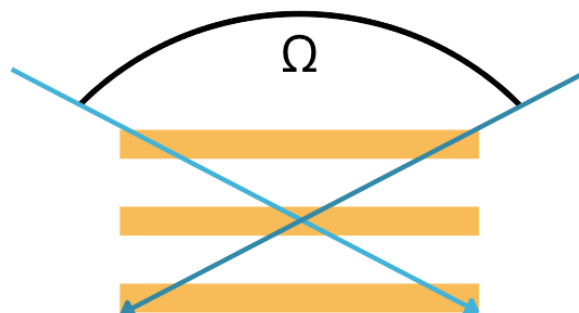

Figure 5-8. Schematic of the hodoscope's maximum field of view (FoV or solid angle) Ω.

Essentially, every position of the hodoscope produces a 3D point cloud after a 12-to-72-hour exposure (for practical reasons, either around 48 h or 72 h were chosen), which has

its own noise. Every time the hodoscope is repositioned, we can produce a new 3D point cloud. These 3D point clouds need to be stitched together, but since this cannot necessarily be done from the information in the existing 3D point clouds (there may be noise that would confuse the algorithms), we need to know the exact position in space of the sensor (hodoscope) that measured the corresponding 3D point cloud.

Therefore, the most important thing here was to fix the position of the different positions with an accuracy of at least +- 1 cm, while +- 1 mm was preferred. The distance from the wall itself does not directly provide any useful information. Every position had to be registered and forwarded to our central computer taking in the measurement data, tied to the exposure done on that position. Absolute and relative dimensions could be used as long as the 1 cm (1 mm) accuracy held up – with the latter, an anchor points (markers) were used on the hodoscope (see Figure 2-1 again), which would allow the semi-automatic lidar to record the position of the hodoscope in the space under the reactor.

The initial on-site measurement with ALARA's hodoscope were carried out at the end of March 2023 and its results helped us to define the parameters for the following tomographic measurements and reliable localization mechanism. For a more detailed plan, please see Table 5-1 in the following page that indicates the following expected timeline. This timeline took 20% unexpected holdups into account, which should mitigate any issues that ought to rise during our development or measurement phases.

Table 5-1. Expected timeline for hodoscope & software development, on-site measurements, data analysis and reporting

Work breakdown	April '23	May 2023					June 2023				July 2023				August 2023					September 2023				October 2023				November 2023				
WEEK NUMBER	17	18	19	20	21	22	23	24	25	26	27	28	29	30	31	32	33	34	35	36	37	38	39	40	41	42	43	44	45	46	47	48
Software improvement	x	x	x	x	x	x	x	x											x	x	x	x	x	x	x							
HMS	x	x	x	x																												
Hodoscope calibration	x	x	x																													
Transportation to Site 1 & Site 2	x		x			x														x												
Measurement at Site 1 (346A)	x	x	x	x	x	x	x	x	x	x	x	x	x	x	x	x	x	x	x													
Removal at Site 1																				x												
Measurement at Site 2 (346B)							x	x	x	x	x	x	x	x	x	x	x	x	x													
Removal at Site 2																				x												
Data analysis	x	x	x																	x	x	x	x	x	x	x	x					
Reporting																								x	x	x	x	x	x	x	x	x

6 FIELD WORKS

On-site measurement activities commenced in early May for reactor 346A and early June for reactor 346B, extending until the commencement of September. Subsequent scanning operations were conducted at reactor 346B over a three-week period from October 30, 2023, to November 22th, 2023.

The measurements were conducted utilizing two hodoscopes, namely H1 for the 346B reactor and H2 for the 346A reactor. In order to obtain the necessary positional metadata for combined reconstruction, the Leica RTC360 LIDAR scanner was employed, as illustrated in Figure 6-1. The Leica RTC360 is a professional-grade LIDAR scanner known for its precision, with a measurement accuracy of 1.9 mm.

Given that the measurement area for reactor 346A comprises three distinct rooms, a total station was utilized to integrate all rooms into a unified logical space. To ensure the accurate capture of hodoscope locations, targets were strategically installed in each room and on each side of the hodoscope. The acquisition of precise hodoscope location data is crucial for effectively stitching together all individual positional data.
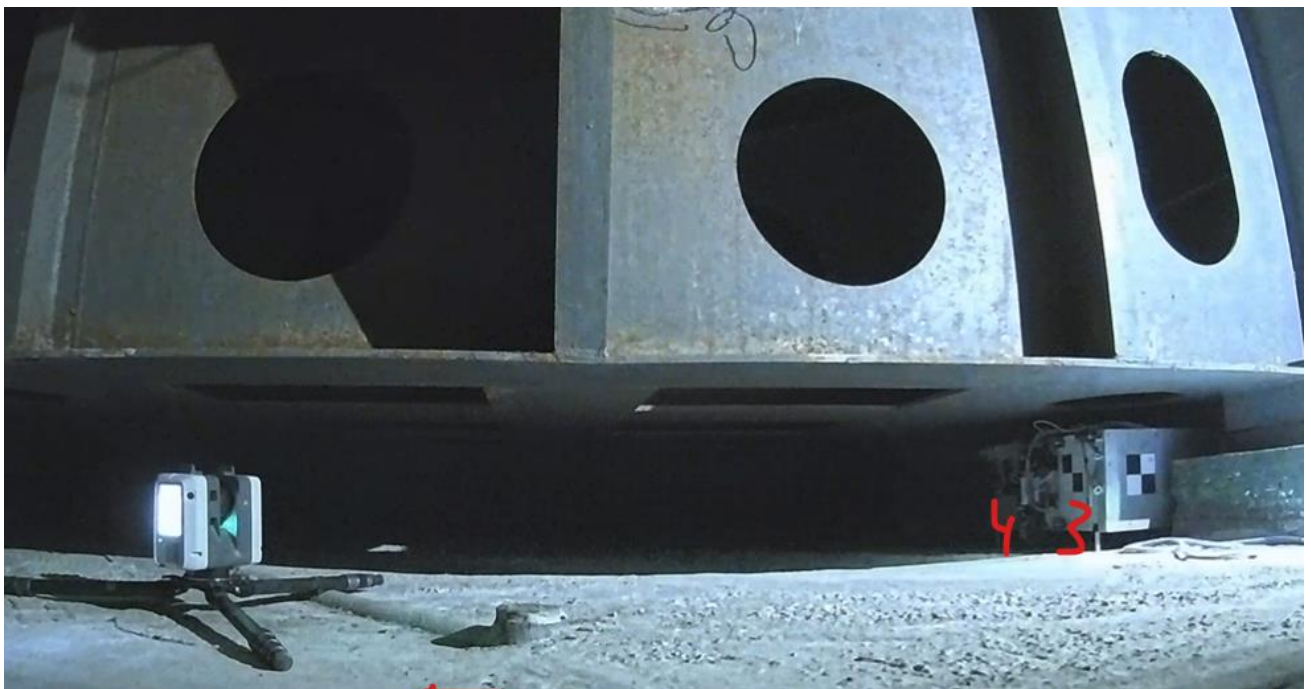
Figure 6-1. A Leica RTC360 operation and positional targets visible on the sides of hodoscope at the main room under the 346A reactor.

6.1 346A reactor measurement statistics

The measurement activities occurred from May 3rd to September 22nd, 2023, encompassing a total of 55 distinct positions during this period. The positioning of these locations at the floor level is depicted in Figure 6-2. Additionally, 8 positions at elevated and tilted angles were scanned in the main room beneath the reactor core. A scanning sequence

of 2-2-3 days per week was employed for positional relocation, conducted manually by the onsite operator.
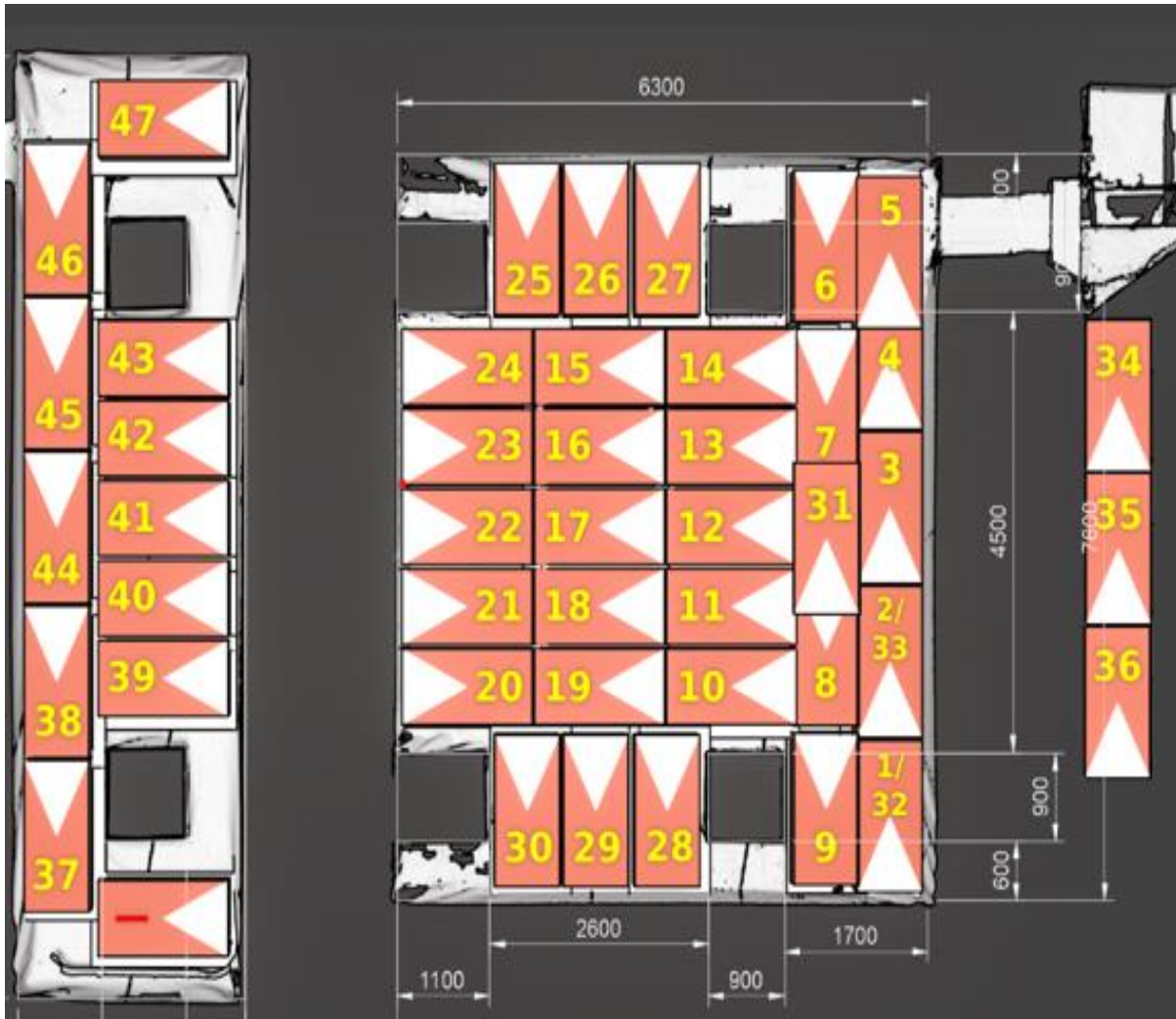

Figure 6-2. Actual measurement plan of 346A reactor. The black triangles represent the 180-degree rotation of positions 31 to 33.

Throughout the duration of the project, nearly 2,700 hours of raw data were collected, resulting in an average effective scanning time of 41 hours per square meter. The cumulative volume of raw data gathered amounted to 122 terabytes. The continuous data rate exhibited variation, ranging from 2.5 gigabytes per hour to 230 gigabytes per hour. The elevated data rate was associated with the level of gamma radiation in specific positions, particularly those directly beneath the reactor core. It is noteworthy that gamma ray tracks were clearly discernible and effectively filtered out during the subsequent data processing phase.

6.2 346B reactor measurement statistics

Measurement works took place from 10th of June until 25th of August 2023. Unfortunate data loss occurred during the data processing which needed to be re-acquired (most of the positional data was lost). Remeasurement took place from 30th October until 22th of November 2023.

During the period 31 different positions were scanned in total. Figure 6-3 shows the placement of positions at the floor level. 2-2-3-day weekly scanning sequence was used for positional relocation. Relocations were done manually by onsite operator. In total 1541 hours of raw data was gathered and out of that 1176 hours' worth of data was lost in the data loss incident. During the remeasuring 1100 h of data was acquired.
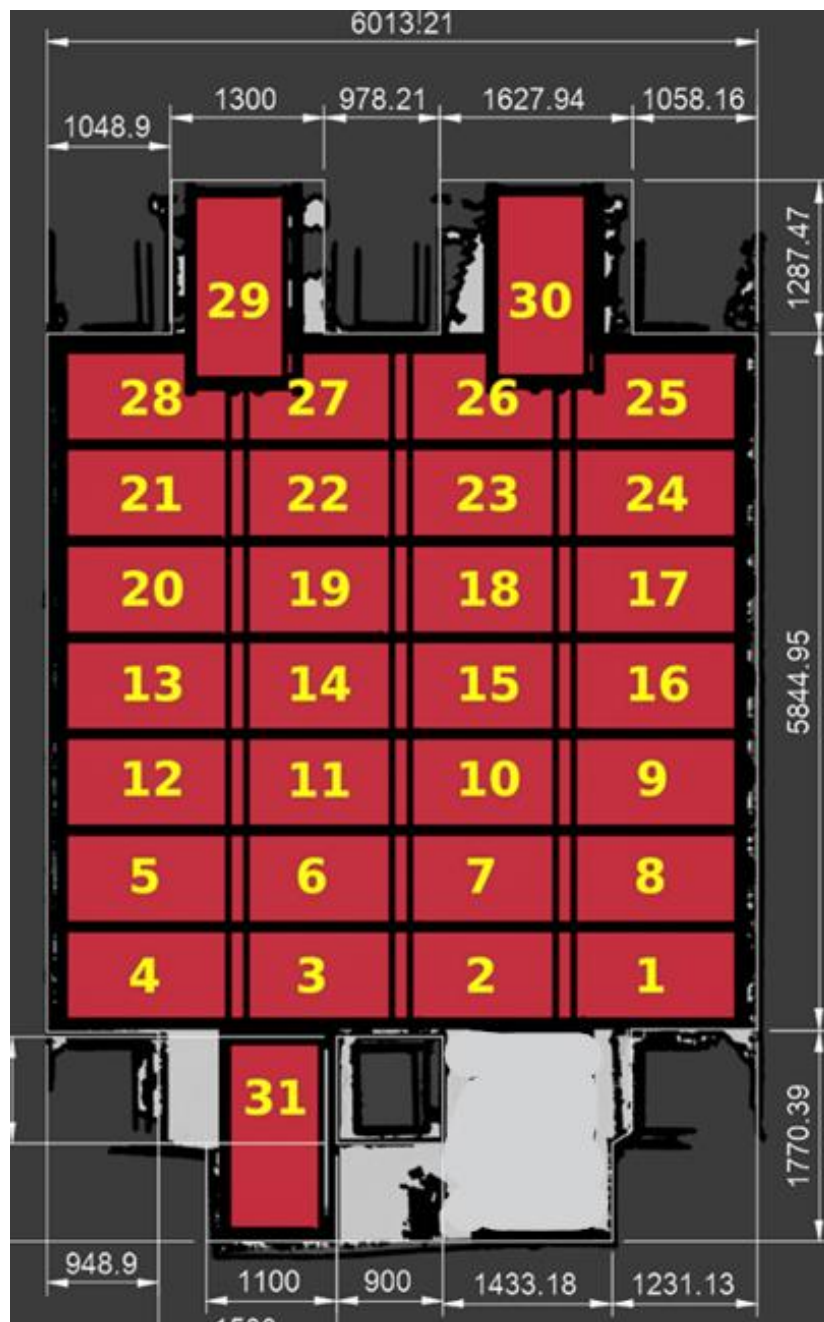
Figure 6-3. Actual measurement plan of 346B reactor.

Amount of raw data gathered in total was 30 TB. Continuous data rate varied from 10 GB/h to 40 GB/h. Comparing to 346A reactor the gamma radiation level was much lower and more even. Also, all positions were in the same room. Average effective scanning time per 1 m^2 was 41 hours.

7   RECONSTRUCTION PROCESS

7.1   Reconstruction and voxel size

For producing one large reconstruction from solitary positional data, a global metadata was created based on LIDAR positioning. Positional metadata was used to transform muon tracks from a single hodoscope active area coordinate into the global coordinates' system.
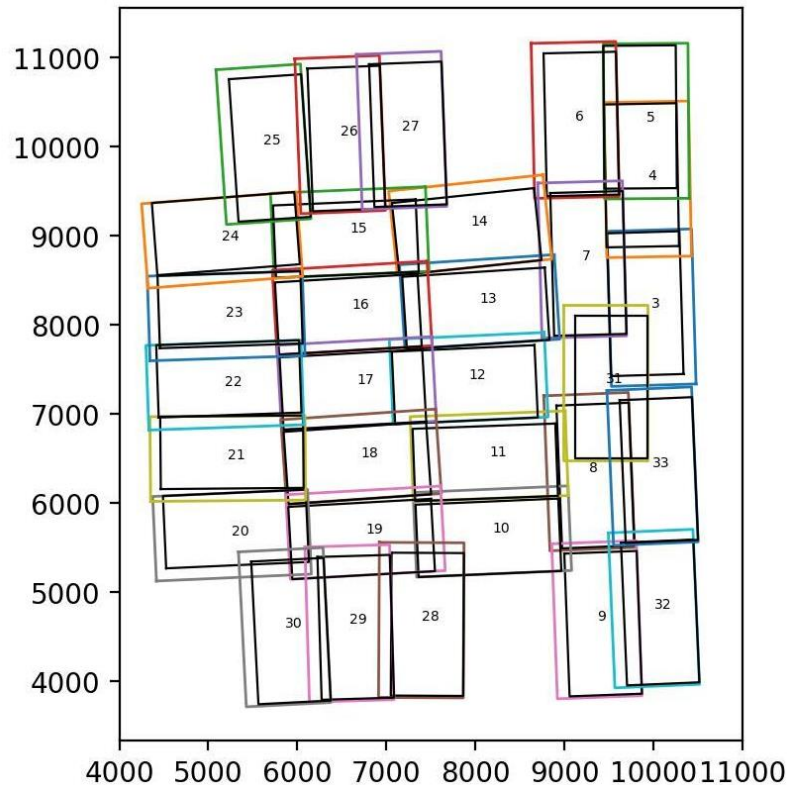
Figure 7-1. Example of 346A actual positions with black rectangles representing the active area and the colored rectangles representing the external dimensions of the hodoscope.

Initial reconstructions were conducted. In Figure 7-2, you can observe the identical volume-of-interest (VOI) with a cross-sectional area of 10 by 7.5 meters, featuring three distinct voxel sizes of 30, 10, and 5 centimeters. None of the aforementioned sizes proved adequate for identifying objects due to insufficient detail and the absence of clear contours, which is why a smaller voxel size — 1 cm — was chosen.
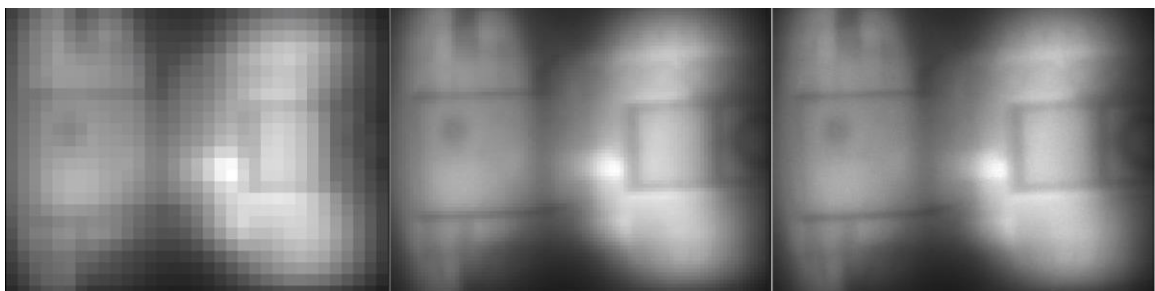
Figure 7-2. Reconstruction with 30 cm, 10 cm and 5 cm voxel sizes at height 3 m. VOI size is 10.0 x 7.5 m.

7.2 Reconstruction of 346A

Reconstruction of 346A Volume of Interest (VOI) sizes were 14m*8m*10m (l*w*h) and was done with 1cm voxel size. Z plane slices were chosen for evaluation providing most visible information. ALARA provided 3D model appears to be precise. Internal structure and the setup of the equipment matches to the reconstruction. Slice numbering is starting from 0-1000, representing slice height from the floor level in centimeters. Lowest point of submarine hull is starting from slice 180. In order to get distance from the lowest point of submarine hull to desired object or height the offset value of 180 must be subtracted from the slice height.
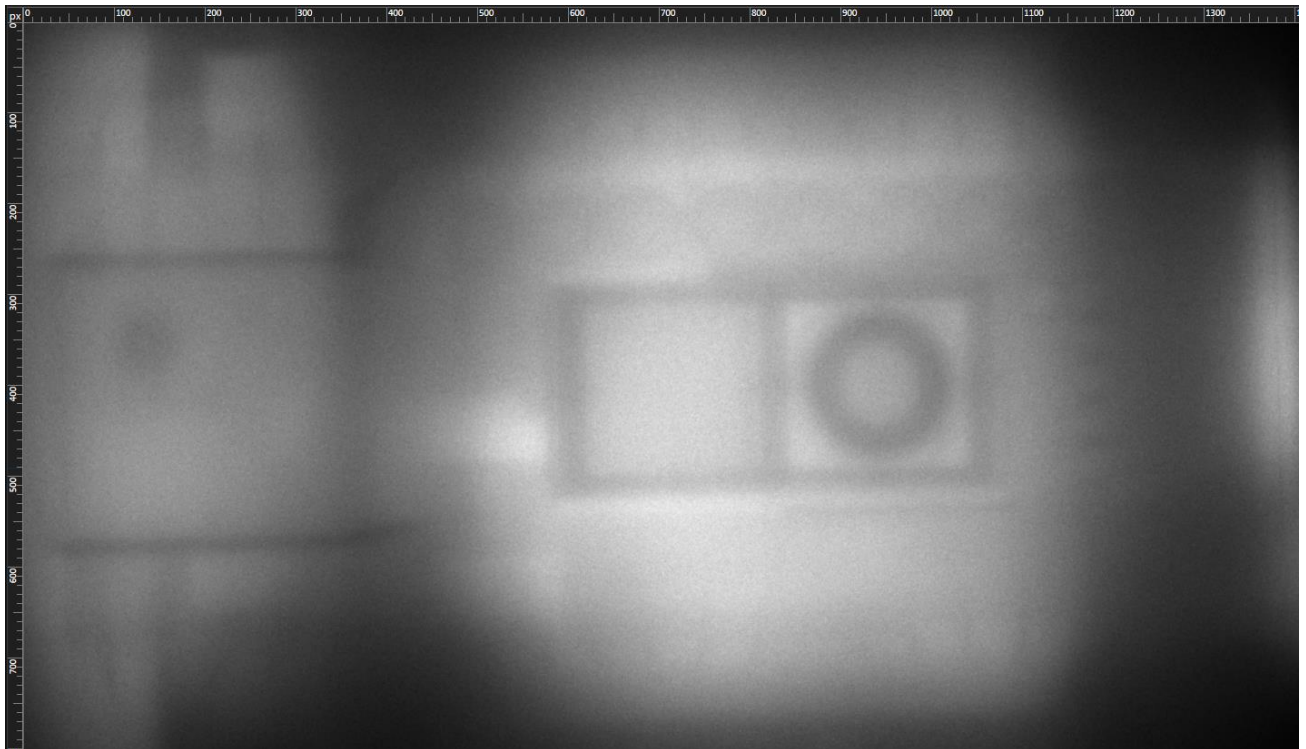
Figure 7-3 VOI of 346A reactor, size 14 x 8 m at height of 3 m, voxel size is 1 cm
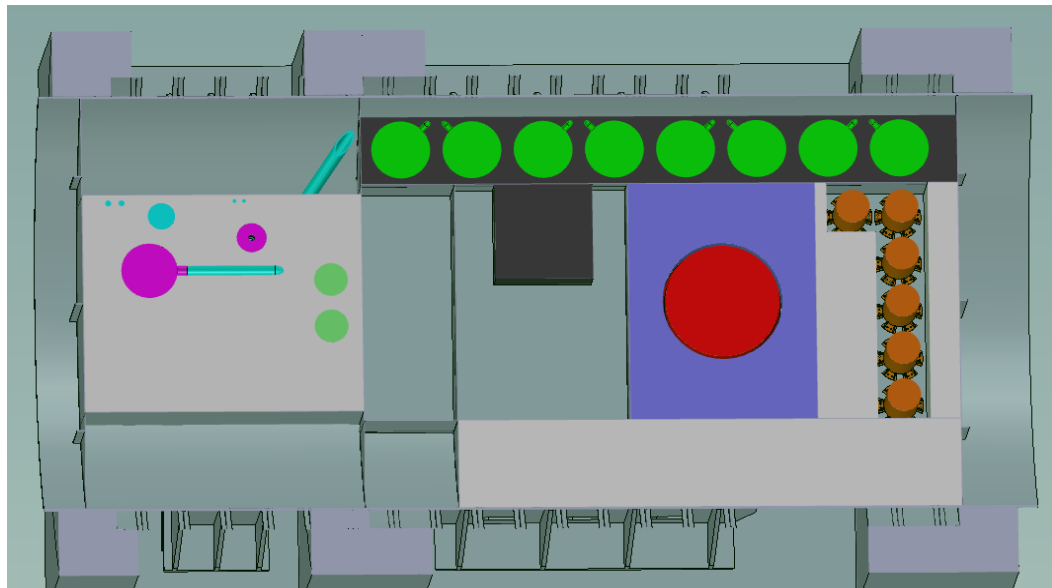
Figure 7-4 Existing 3D model of 346A reactor, Z plane cut at ~ 3 m

List of all identified objects not defined or present in the current 3D model. All objects on the list are added to the 3D model with designated reference number of FO-xxx (Found Object). All object measures are approximate. Picture 1 pixel/voxel = 1 centimeter

Table 7-1. 346A found objects list

No	Ref No	Location	Description
1.	FO-001	U-shape room	Less dense area with size 150x100x 60cm, slice 210-270
2.	FO-002	U-shape room	Less dense area size 60x60x60cm, slice 220-280
3.	FO-003	U-shape room	Turbine lower section with piping, denser, slice 210-250
4.	FO-004	U-shape room	Group of denser objects in various shapes and sizes, slice 220-270
5.	FO-005	On top of U-shape room	Concrete filling, partially filled, model corrected, slice 420-530
6.	FO-006 FO-006_2	Reactor lid	L shape denser object around reactor lid 160x60x150/ 60x130x150cm, slice 590-740
7.	FO-007	Reactor lid	Dense object 50*50*80cm, slice 610-690
8.	FO-008	Reactor lid	Dense object 150*80*100cm, slice 620-720
9.	FO-009	Port side	Pipes, 5 pcs, Ø15cm h=90-100cm, 460-550
10.	FO-010	Near reactor lid	Round denser object Ø60cm, h=45cm, slice 590-635
11.	FO-011	Left to side	Group of 4 denser objects, Ø20-40cm, slice 520-560
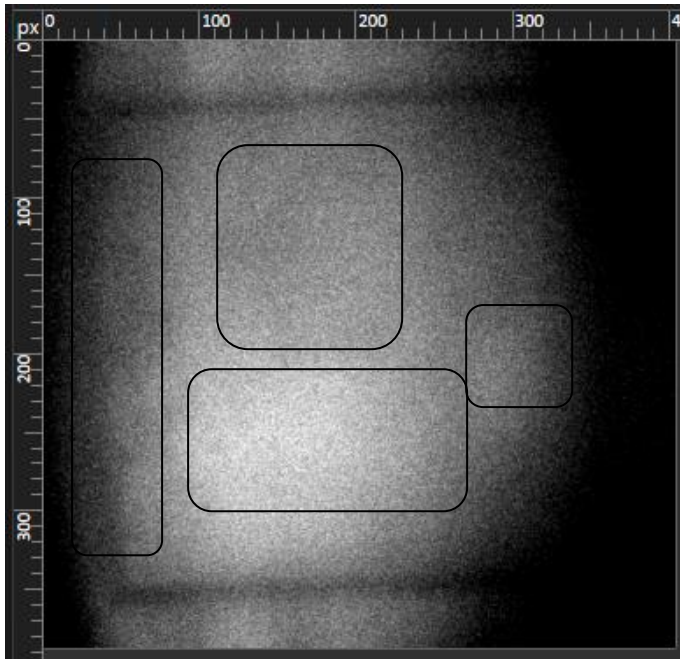
Figure 7-5 U-shape room with objects, slice240

Most of the objects were found from the U-shape room from height of 200-280 which largely matches with waste emplacement description. Two less dense areas could be paraffin containers with neutron sources. Turbine lower section with piping is visible in the upper middle part of figure 7-5. By the left wall, couple of denser areas are recognizable.

The room on top of U-shape is partially filled with concrete which is clearly visible in the figure 7-6. Darker area is the turbine.
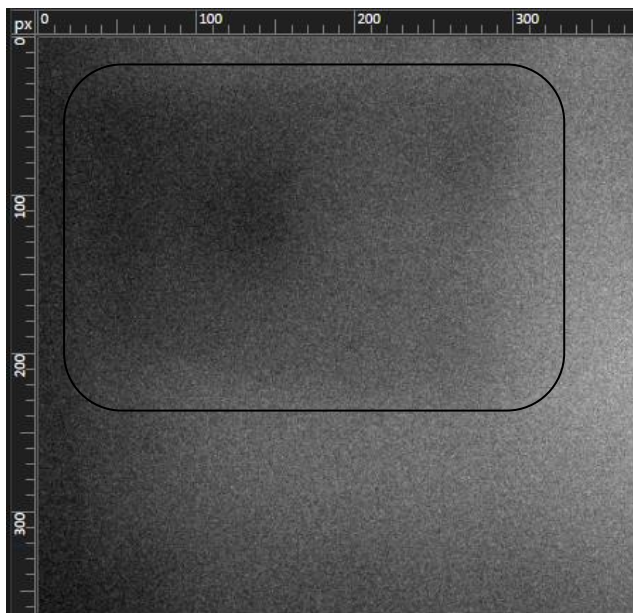
Figure 7-6 Room on top of U-shape room half-filled with concrete slice 475
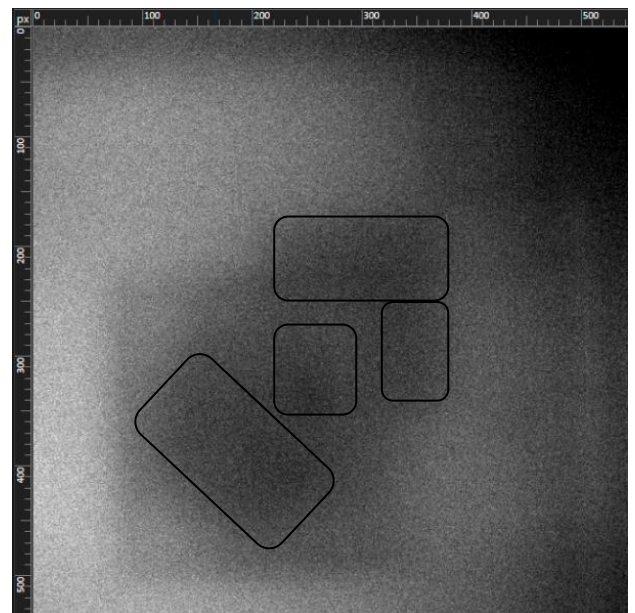
Figure 7-7 Reactor lid area. Slice 640

There are many objects in the area around and on the reactor lid (see figure 7-7). Dense flipped L shape object around the reactor lid. Very dense objects on top of reactor lid could be the steel/lead containers for Co-60. Concrete covered hatch is clearly visible on the upper right corner and corresponds with existing 3D   model.

Port side of the submarine (see figure 7-8) revealed a round shaped hollow object, most probably pipes with Ø15cm. Lower ones on top of steam generator. Upper ones are near to submarine hull wall. Visible length ~1m.
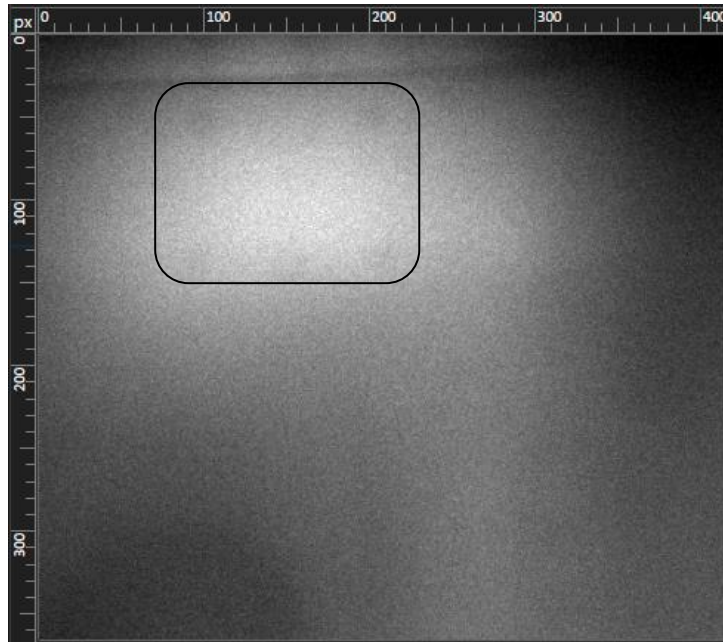

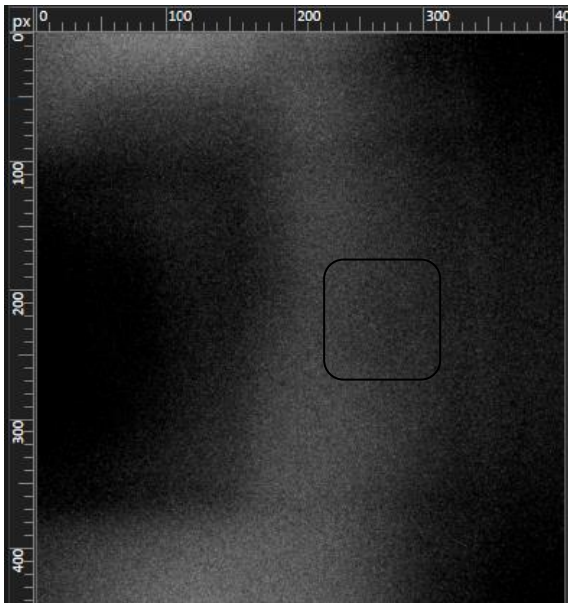Figure 7-8 Five pipes *Ø15cm slice 500*
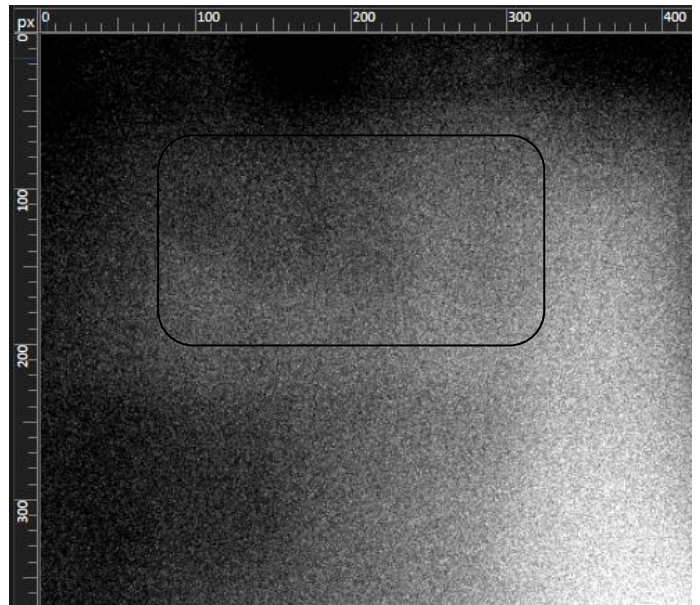

Figure 7-9 Round object on the right of reactor, slice 610

Figure 7-10 Group of 4 objects, slice 530

Round object in the room on the right of reactor lid (see figure 7-9). Diameter 60cm, h=50cm. In figure 7-10, round objects with diameter 20-40cm, h=40cm.
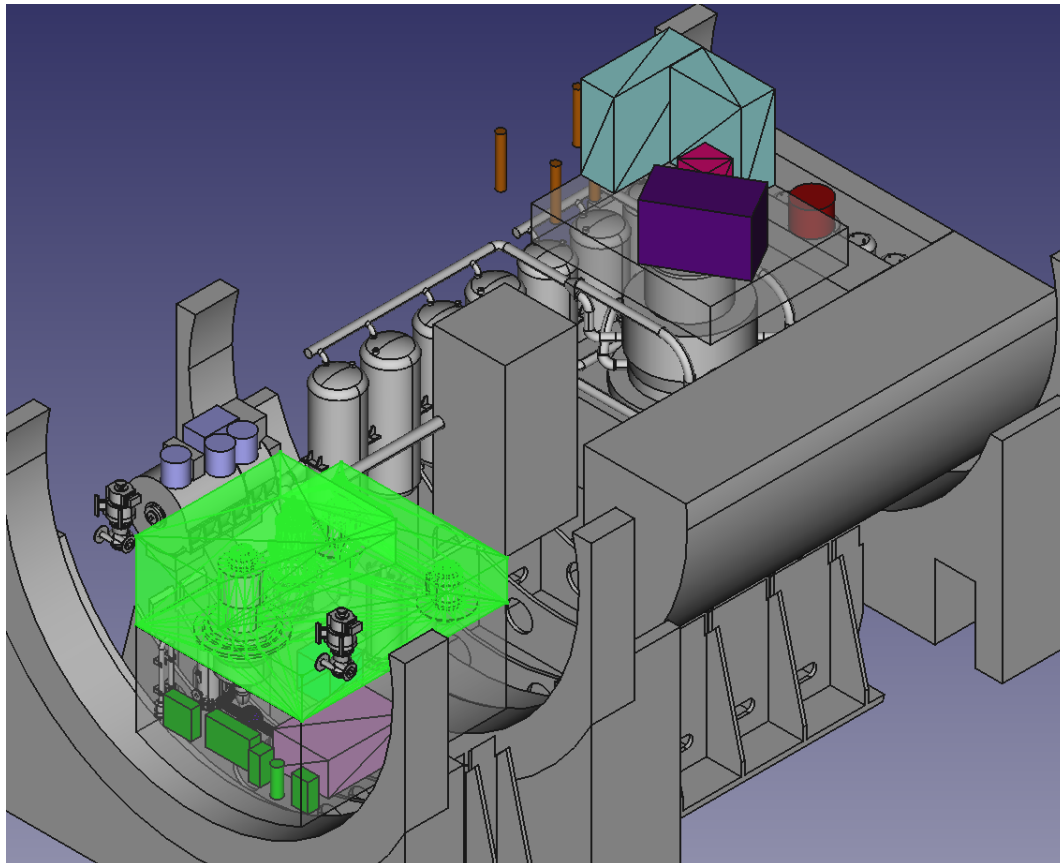
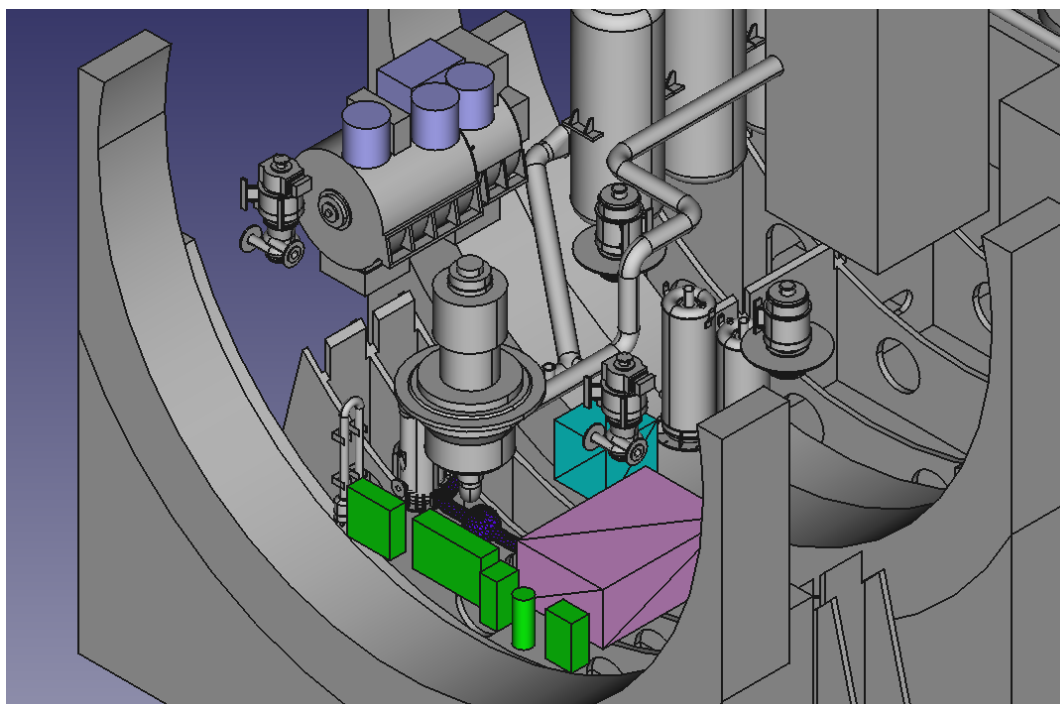Figure 7-11 Volumetrically defined findings layer in the existing 3D model of 346A

Figure 7-12 Defined findings in the lower section of U-shape room of 346A
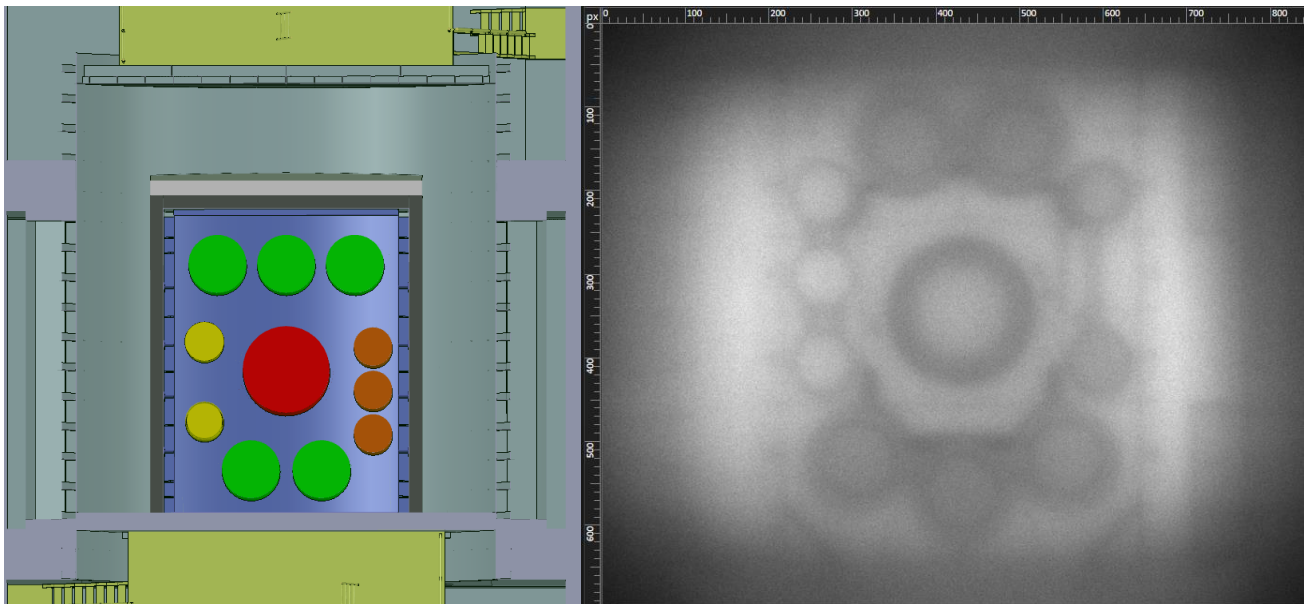
7.3. Reconstruction of 346B

Figure 7-13 346B existing 3D model and tomographic reconstruction, z plane at ~3m. Listed deviations a; b; c; d; e and f are clearly visible.

Reconstruction of 346B Volume of Interest (VOI) sizes were 10m*9,5m*10m (l*w*h) and was done with 1cm voxel size. Z plane slices were chosen for evaluation providing most visible information. There are major deviations in the 3D model compared to the reconstruction.

Slice numbering is starting from 0-1000, representing slice height from the top of hodoscope active area in centimeters. Lowest point of submarine hull is starting from slice 155. In order to get distance from the lowest point of submarine hull to desired object or height the offset value of 155 must be subtracted from the slice height.

List of structural deviations:

a) Reactor compartment is oriented 180 degree the other way around;

b) Presence of internal reactor shield tank and dense lining around steam generators (probably lead);

c) Radial placement of steam generators;

d) Reactor compartment bow side corners cut off, dense lining;

e) Additional equipment in reactor compartment stern side corners;

f) Three separate rooms in port side 1st deck, two filled with concrete;

g) Port and starboard biological shields are shorter and in one piece. At height 360-600;

h) The length of port and starboard 2nd decks is same as the reactor compartment and does not extend further to the stern;

i) Inside top biological shield, multiple denser areas visible, possibly circuit pump and valve units.
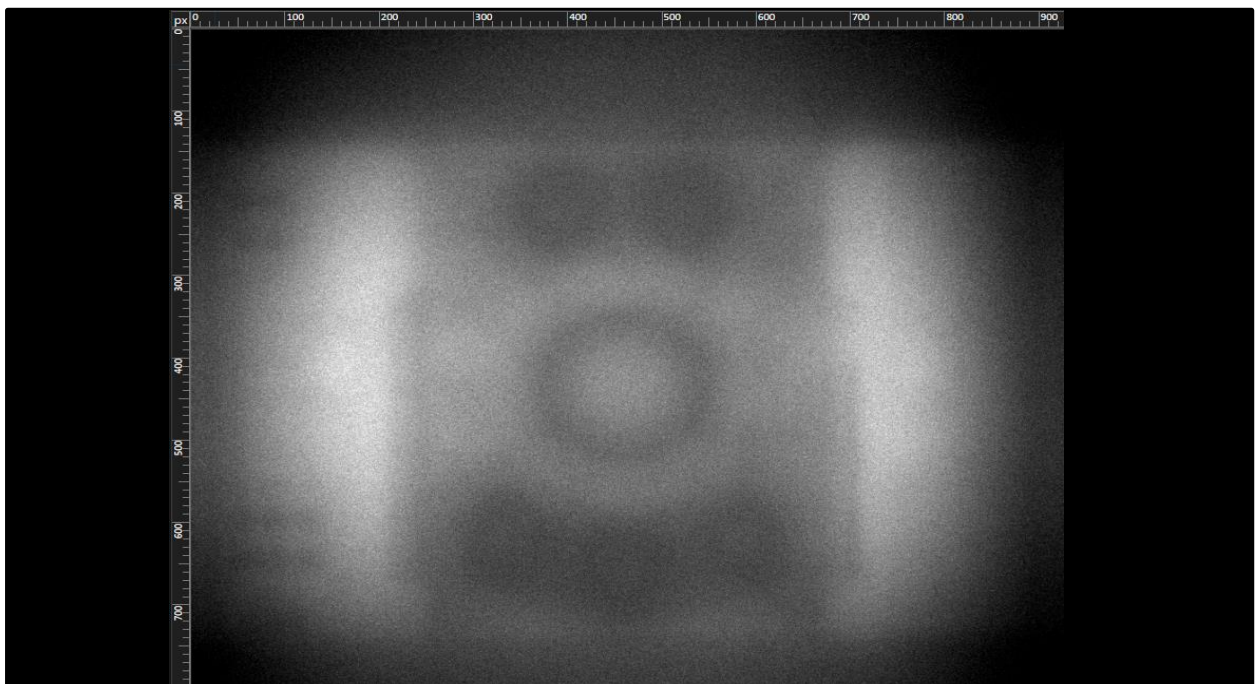

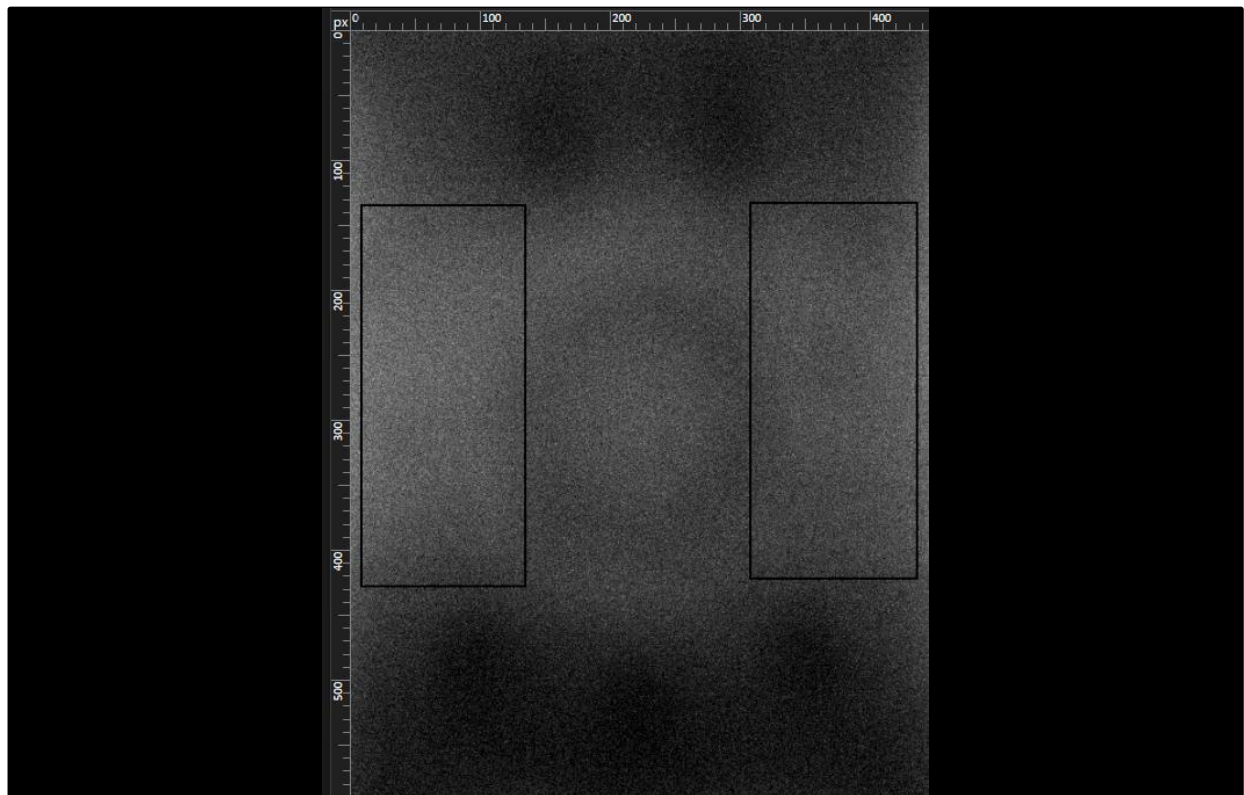Figure 7-14 Slice 500, 2nd deck (h) and side biological shields (g).

Figure 7-15 Slice 580, reactor compartment, inside the top biological shield multiple objects are visible.

List of all identified objects not defined or present in the current 3D model. All objects on the list are added to the 3D model with designated reference number of FO-xxx (Found Object). All object measures are approximate.

Table 7-2. 346B found objects list

| No	Ref No	Location	Description
1.	FO-001	Starboard side, 2nd deck	Cluster of 4 round denser objects Ø20cm, 470-slice 640
2.	FO-002	Starboard side, 2nd deck	Cluster of 6 round denser objects Ø20cm, 470-slice 640
3.	FO-003	Starboard side, 2nd deck	Irregular shape less dense object Ø70cm, slice 520-560
4.	FO-004	Starboard side, 2nd deck	Irregular shape less dense object Ø100cm, slice 520-560
5.	FO-005	Starboard side, 2nd deck	2 round denser object Ø30cm, slice 530-560
6.	FO-006	Port side, 2nd deck	2 irregular shape less dense objects, Ø60cm, slice 520-560
7.	FO-007-01 FO-007-02	Poured concrete top	A group of denser areas inside poured concrete slab on top reactor, 250x80cm and 150x60cm, slice 650-700
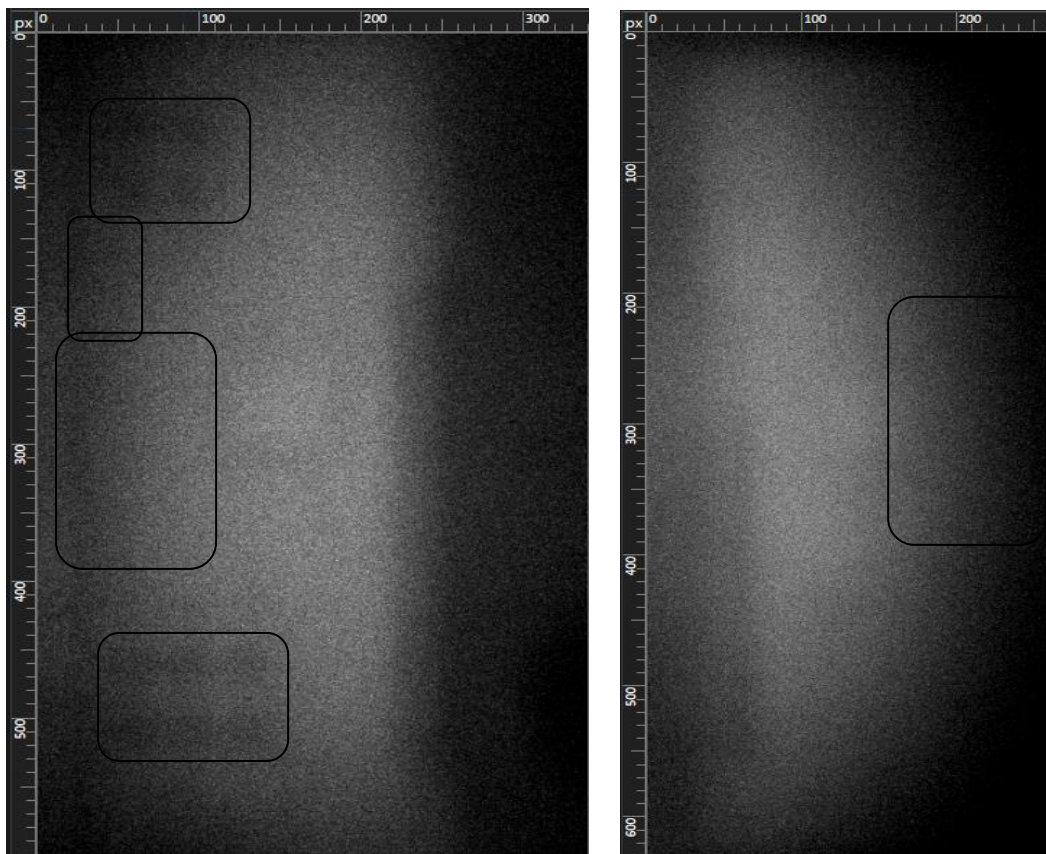
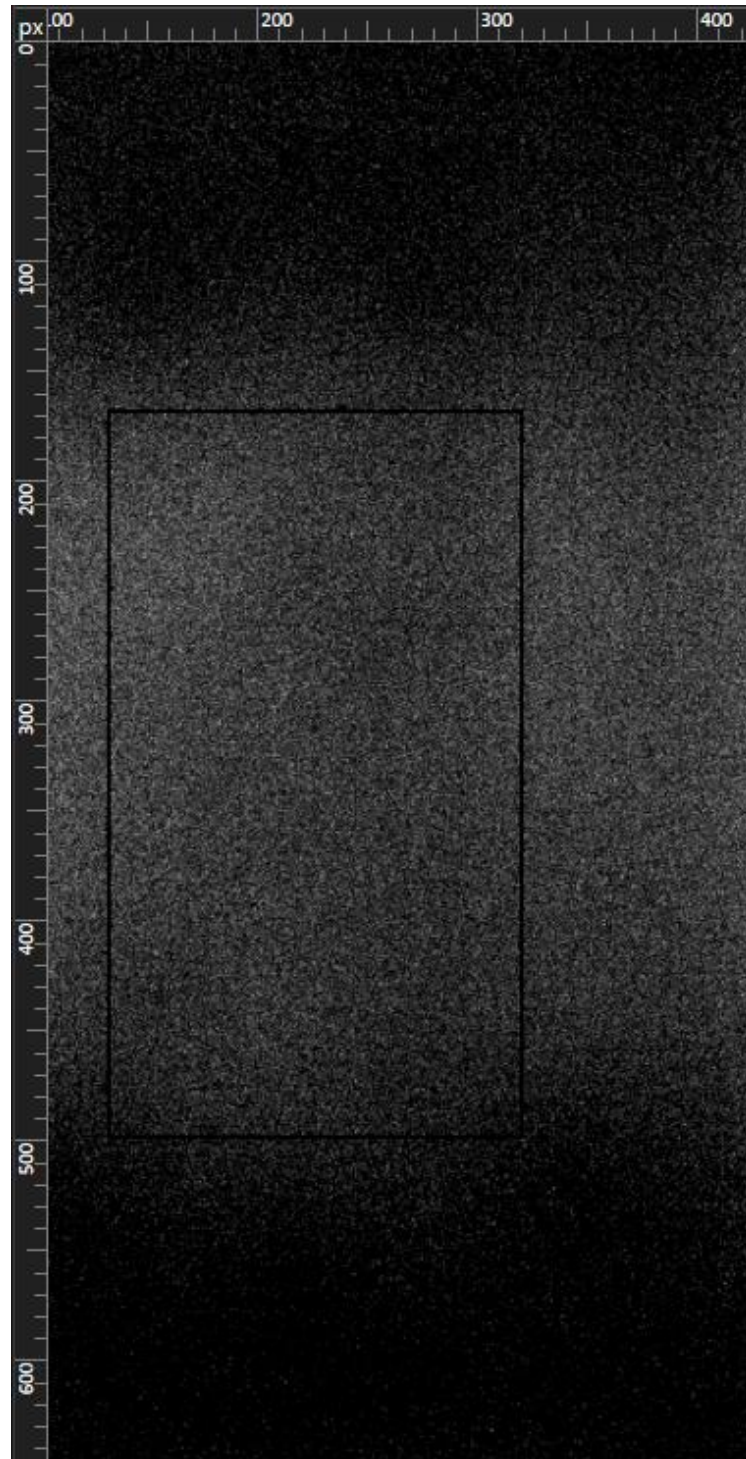Figure 7-16 Starboard side, slice 540.

Figure 7-17 Slightly denser area on top of reactor inside the poured concrete layer. Slice 680.
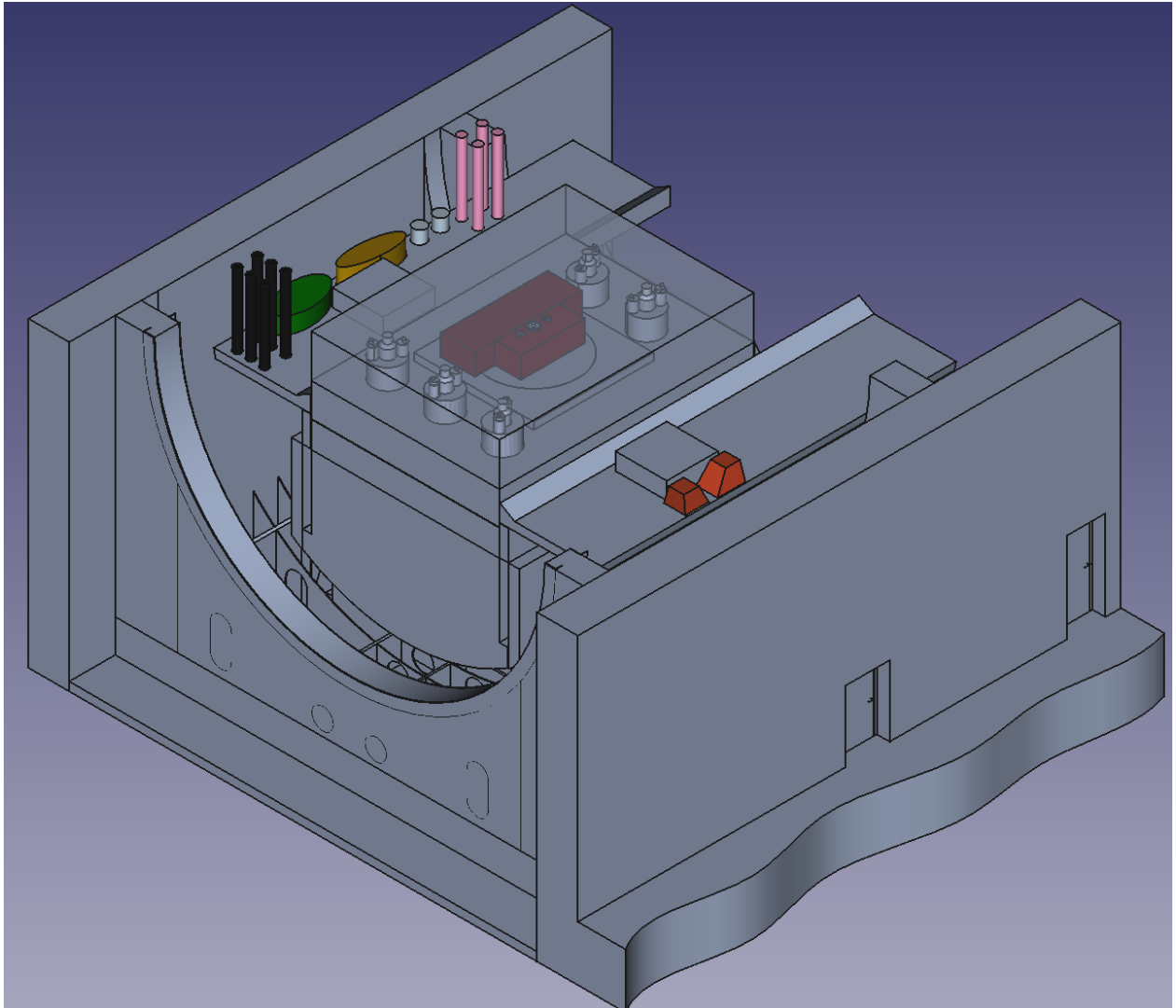
Figure 7-18 Volumetrically defined findings layer in the existing 3D model of 346B